JNeurosci
THE JOURNAL OF NEUROSCIENCE

Research Articles | Development/Plasticity/Repair

PTPRO restricts higher-order branching of terminal arbors through TrkB dephosphorylation

https://doi.org/10.1523/JNEUROSCI.0713-26.2026

Received: 29 April 2026
Revised: 26 September 2026
Accepted: 23 October 2026

Copyright © 2026 the authors

This Early Release article has been peer reviewed and accepted, but has not been through the composition and copyediting processes.The final version may differ slightly in style or formatting and will contain links to any extended data.

Alerts: Sign up at www.jneurosci.org/alerts to receive customized email alerts when the fully formatted version of this article is published.

PTPRO restricts higher-order branching of terminal arbors through TrkB dephosphorylation

Abbreviated title: PTPRO Restricts Terminal Arbor Branching via TrkB

Jiaxuan Li[1,2], Misato Yasumura[2,3], Tokuichi Iguchi[4,5,6], Manabu Taniguchi[2], Yuichiro Oka[2,4], Chao-Yuan Tsai[2], Makoto Sato[1,2,4,7]*

[1]Graduate School of Frontier Biosciences, The University of Osaka, Osaka, Japan

[2]Department of Anatomy and Neuroscience, Graduate School of Medicine, The University of Osaka, Osaka, Japan

[3]Division of Radioisotope and Radiation Research, Life Science Research Center, University of Toyama, Toyama, Japan

[4]Division of Developmental Neuroscience, Department of Child Mental Development, United Graduate School of Child Development (UGSCD), The University of Osaka, Osaka, Japan

[5]Laboratory of Anatomy and Physiology, Graduate School of Health Sciences, Fukui Health Science University, Fukui, Japan

[6]Department of Applied Chemistry and Biotechnology, Graduate School of Engineering, University of Fukui, Fukui, Japan

[7]Lead contact

*Correspondence: sato.makoto.med@osaka-u.ac.jp

Number of pages: 43

Number of figures: 7

Number of supplemental figures: 6

Number of words for abstract: 146

Number of words for introduction: 533

Number of words for discussion: 1347

Conflict of interest statement: The authors declare no competing interests.

JNeurosci Accepted Manuscript

Author contributions

Conceptualization, J.L., M.Y., and M.S.; performed experiments, J.L., M.Y., T.I., M.T., and Y.O.; provided expertise and feedback, M.Y., T.I., M.T., Y.O., C.-Y.T., and M.S.; wrote the manuscript, J.L. together with M.Y., T.I., and M.S. All authors reviewed and approved the manuscript.

Acknowledgments

We thank all laboratory members for their helpful discussions and support. We thank M.-Y. Ma for assistance with neuronal cultures, and Q. Yang for helpful discussions on the experiments. We are grateful to the University of Osaka for providing access to microscopy services and technical assistance. We also thank the Center of Medical Innovation and Translational Research (CoMIT) for performing the sequencing. This work was supported by the Japan Society for the Promotion of Science (JSPS KAKENHI grant numbers JP24K09667 to Y.O., JP25K09834 and JP22K06458 to M.Y., and JP20H03414 to M.S.) and by JST SPRING (grant number JPMJSP2138).

JNeurosci Accepted Manuscript

Abstract

The structural complexity of axon collateral terminal arbors shapes synaptic connectivity. In corticospinal projections, individual axon collaterals exhibit distinct patterns of terminal arborization, ranging from sparse local branches to dense, highly complex arbors in target regions such as the pontine nuclei. How this complexity is controlled remains poorly understood. Here, using corticopontine projections in male and female mice, we show that protein tyrosine phosphatase receptor type O (PTPRO) selectively restricts higher-order branching of terminal arbors in the pontine nuclei without affecting collateral number. This function requires the intracellular phosphatase domain of PTPRO but not its extracellular region. We demonstrate that PTPRO dephosphorylates tropomyosin receptor kinase B (TrkB), and that the excessive terminal arborization caused by acute PTPRO loss is rescued by TrkB depletion or phosphatidylinositol 3-kinase (PI3K) inhibition. Together, these findings reveal that PTPRO-mediated TrkB dephosphorylation acts as a molecular brake on corticopontine terminal arbor elaboration.

JNeurosci Accepted Manuscript

Significance Statement

How individual axons regulate terminal branching within target regions is a fundamental question in neural circuit development. This study identifies protein tyrosine phosphatase receptor type O (PTPRO), a receptor-type protein tyrosine phosphatase that negatively regulates signaling through tyrosine phosphorylation, as a selective regulator of higher-order branching in corticopontine terminal arbors. PTPRO dephosphorylates tropomyosin receptor kinase B (TrkB), a neurotrophin receptor tyrosine kinase that promotes neuronal growth and branching, thereby restricting terminal arbor complexity without affecting collateral number from the main axon. Given that terminal arbor architecture determines the synaptic territory of each cortical input, PTPRO-dependent constraint on arbor elaboration may represent a general principle by which projection-specific arbor complexity is established across long-range circuits in the central nervous system.

JNeurosci Accepted Manuscript

Introduction

Terminal arborization represents the final stage of axonal development, during which collateral branches elaborate into complex, synapse-bearing structures within target regions. The geometry of these arbors directly determines the functional properties of the resulting neural circuits (Bastmeyer and O'Leary, 1996; Winnubst et al., 2019). In corticopontine projections, layer 5 pyramidal neurons form elaborate terminal arbors within the pontine nuclei that are essential for cerebro-cerebellar communication (O'Leary and Terashima, 1988; Bastmeyer and O'Leary, 1996; Kalil and Dent, 2014). These arbors exhibit striking heterogeneity. Motor cortex-derived axons form compact, high-density terminal fields, whereas associative cortical inputs develop more dispersed branching patterns (Leergaard and Bjaalie, 2007). Collateral branches first extend into pontine neuropil, followed by iterative elaboration of higher-order terminal branches (Mihailoff et al., 1984; Bastmeyer and O'Leary, 1996). Such diversity suggests that arborization complexity is precisely regulated to meet the specific computational demands of different cortical inputs, yet the underlying molecular mechanisms remain poorly understood. In our previous study, we showed that corticospinal tract axons from distinct cortical areas extend collateral branches to corresponding pontine subregions, forming a region-to-region corticopontine projection, but the mechanisms that shape their terminal arborization remain poorly understood (Iguchi et al., 2021).

The final architecture of a terminal arbor emerges from the balance between growth-promoting and growth-restricting signals (Sato et al., 1994). Brain-derived neurotrophic factor (BDNF) acting through tropomyosin receptor kinase B (TrkB) and the downstream phosphatidylinositol 3-kinase (PI3K)–Akt cascade promotes branch formation and arbor elaboration (Jaworski et al., 2005; Cohen-Cory et al., 2010). Conversely, phosphatase and tensin homolog (PTEN) antagonizes PI3K–Akt signaling to limit arbor overgrowth (Kwon et al., 2006). However, these studies have primarily addressed initial collateral outgrowth or overall arbor size. The intrinsic mechanisms that specifically control higher-order branching complexity remain largely unknown.

Receptor-type protein tyrosine phosphatases (RPTPs) negatively regulate receptor tyrosine kinase signaling and represent plausible candidates for such regulation (Stoker, 2001; Johnson and Van Vactor, 2003). In *Drosophila*, the RPTP PTP69D acts together with Slit to regulate the spatial patterning of axon

JNeurosci Accepted Manuscript

branching via Dscam1 (Dascenco et al., 2015). However, these studies were performed in invertebrate sensory neurons and primarily addressed branch targeting rather than the hierarchical complexity of terminal arbors. Therefore, whether RPTPs play analogous roles in regulating terminal arborization complexity in the mammalian central nervous system remains unexplored. PTPRO is a type III RPTP containing a single intracellular catalytic domain and extracellular fibronectin type III-like domains (Krueger and Saito, 1992; Tagawa et al., 1997; Tautz et al., 2013). It has been implicated in axon growth and guidance in the peripheral nervous system (Tagawa et al., 1997; Stepanek et al., 2001). In trigeminal ganglion neurons, PTPRO restricts axon growth and branching by dephosphorylating TrkB (Gatto et al., 2013). However, that study examined overall axon elongation and branching in sensory neurons, leaving open whether PTPRO can selectively regulate higher-order terminal arborization in central projection systems and through which downstream signaling pathway.

Here, we investigated the role of PTPRO in corticopontine terminal arborization. We found that PTPRO restricted higher-order branching of corticopontine terminal arbors through phosphatase-dependent inhibition of TrkB-PI3K signaling. These findings reveal a cell-intrinsic brake on terminal arbor complexity and extend PTPRO-TrkB regulation from general axon growth control to the structural refinement of central projection terminals.

JNeurosci Accepted Manuscript

Materials and Methods

Animals

All animal experiments were conducted in compliance with the Regulations on Animal Experimentation at the University of Osaka and approved by the Animal Experimentation Committee of the University of Osaka. The animals were kept under a 12-h light/12-h dark cycle. They were allowed to feed and drink ad libitum. ICR mice were purchased from Japan SLC Inc. The day of confirmation of a vaginal plug was designated as embryonic day 0.5 (E 0.5). The day of birth was designated as postnatal day 0 (P0). Both male and female embryos at E12.5 were used for *in utero* electroporation (IUE). Pups at P1, P2 and P4 were used for tissue processing and imaging. Pups at P0 or P2 were used for *in situ* hybridization (ISH) and immunohistochemistry (IHC).

Plasmid construction

pCAGGS vector (Niwa et al., 1991) was modified to insert multiple cloning sites with a C-terminal 3xFLAG tag to yield pCAGGS-5MCS-FLAG. The coding sequences of mouse PTPRO and TrkB were amplified by PCR with specific primers*:*

5’-CTAGCGGCCGCATGGGGCACCTGCCTAGGGGAAC-3’ and

5’-TCGCTCGAGGGATTTGCTGACGTTCTCGTAGATGACGTCGC-3’ for PTPRO, and

5’-GCGGCGGCCGCATGTCGCCCTGGCTGAAGTGG-3’ and

5’-CCGGAATTCGCCTAGGATATCCAGGTAGACGGG-3’ for TrkB using cDNA prepared from E16 ICR embryos and cloned into the NotI and XhoI restriction enzyme sites of pCAGGS-5MCS-FLAG and the NotI and EcoRI restriction enzyme sites of pCAGGS-5MCS-V5 (Iguchi et al., 2021) vector to yield pCAGGS-PTPRO-FLAG and pCAGGS-TrkB-V5, respectively.

The expression vector for PTPRO substrate-trapping mutant (pCAGGS-PTPRO^{DA}-FLAG) was constructed by site-directed mutagenesis PCR (Aiyar et al., 1996) introducing the aspartic acid to alanine (D1112A) substitution. Briefly, pCAGGS-PTPRO-FLAG vector was used as a template with the primers:

5′-GTGATGCATTTTAACTACACAGCCTGGCCCGCTCACGGCGTGCCTCCAGC-3’

Neurosci Accepted Manuscript

5’-GTCCTCGAGGGATTTGCTGACGTTCTC-3’.

The mutagenic base is underlined. The mutated fragment carrying the NsiI and XhoI restriction enzyme sites was used to replace the NsiI and XhoI fragment in the pCAGGS-PTPRO-FLAG construct to yield the plasmid. The PTPRO lacking the extracellular domains was amplified from pCAGGS-PTPRO-FLAG vector by PCR using primer pairs:

5′-TTGCCACCAGATCTGCGGCCGCATGGGGCACCTGCCTAGG-3’ and

5′-GCACCGAGATCGTCGTAACAATCTTGAGCAGC-3’,

5′-TGTTACGACGATCTCGGTGCTGGCCATC-3’ and

5′-GTCATCCTTGTAGTCCTCGAGGGATTTGCTGACGTTCTCG.

These two PCR products were inserted into the NotI and XhoI restriction enzyme sites of pCAGGS-PTPRO-FLAG vector using In-Fusion HD Cloning Kit (Clontech) to yield pCAGGS-PTPRO^{NTD}-FLAG. The PTPRO lacking the extracellular domains and signal peptides was amplified from pCAGGS-PTPRO-FLAG vector by PCR using primers:

5′-CACCTCGAGATCTCGGTGCTGGCCATCCTC-3’

5′-ACAGCGGCCGCGGATTTGCTGACGTTCTCGTAG-3’.

The PCR product was inserted into the XhoI and NotI restriction enzyme sites of pEB-PPTsp-V5-MCS vector (Nguyen et al., 2022) using Ligation high Ver.2 (TOYOBO CO., LTD.) to yield pEB-PPTsp-V5-PTPRO^{NTD}. Plasmids encoding short hairpin RNA (shRNA) constructs were obtained from the MISSION RNAi Consortium shRNA Library (Sigma-Aldrich). The targets of shRNAs for *Ptpro* were as follows (TRCN0000029984-TRCN0000029988): pLKO.1-sh*Ptpro* #1, 5′-CCAGAGTTGATTCAACAGTTT-3’; pLKO.1-sh*Ptpro* #2, 5′-CGATTCTTACATCAAGGATAT-3’; pLKO.1-sh*Ptpro* #3, 5′-GCGCTCATACCGAATGTCAAT-3’; pLKO.1-sh*Ptpro* #4, 5′-CCATTCACAGAAGAACCCATT-3’; pLKO.1-sh*Ptpro* #5, 5′-CCTACAACAGAAGTCCCACAT-3’. The targets of shRNAs for *Ntrk2* were as follows: pLKO.1-sh*Ntrk2* #1, 5′-GCCTCGAATTACGTGGATGAA-3’; pLKO.1-sh*Ntrk2* #2, 5′-CCTTAAGGATAACGAACATTT-3’; pLKO.1-sh*Ntrk2* #3, 5′-CCACGGATGTTGCTGACCAAA-3’; pLKO.1-

Neurosci Accepted Manuscript

sh*Ntrk2* #4, 5′-GCTTACAAAGCGTTTCTGAAA-3’; pLKO.1-sh*Ntrk2* #5, 5′-CATTCCAAGTTTGGCATGAAA-3’.

The BamHI-HindIII Cre fragment from paavCAG-iCre (Addgene plasmid # 51904) was subcloned into the NheI and HindIII restriction enzyme sites of pEGFP-C1 (Clontech) to yield pCMV-Cre. pCA-mTmG was a gift from Liqun Luo (Addgene plasmid # 26123).

Transcriptomic screening of RPTP genes

Publicly available transcriptomic datasets of corticospinal projection neurons were obtained from the Gene Expression Omnibus (GEO; accession number GSE2039). Expression profiles were analyzed using Subio Platform version 1.19 and Subio Basic Plug-in (Subio Inc. Kagoshima, Japan). RPTP family genes were retrieved from the gene annotation list using the keyword “protein tyrosine phosphatase receptor”. Candidate genes were evaluated using two complementary criteria. The first was a higher processed signal in corticospinal projection neurons than in callosal projection neurons at E18. The second was strong expression at E18, the stage of collateral branch formation, followed by a gradual decrease during subsequent development. Genes meeting both criteria were selected for further functional analysis and subjected to shRNA-mediated knockdown by IUE at E12.5.

RT-PCR

EGFP-expressing L5 cortical neurons were isolated from Tg(*Fezf2*-EGFP)CO61Gsat (Gong et al., 2003) embryos and pups by fluorescence activated cell sorting (Clare et al., 2018). cDNAs were synthesized using total RNA isolated from EGFP-expressing L5 cortical neurons. The PCR primers 5′-AGGTGAACCCTAACGTGGTG-3’ and 5′-GTCCTTGGCCATATCCTTG-3’ were used to detect transcripts of two splice variants (long-form and short-form *Ptpro*) expressed in the CNS.

***In situ* hybridization (ISH) and Immunohistochemistry (IHC)**

Ptpro probe was prepared as follows. cDNA fragment of *Ptpro* was amplified from mouse brain cDNA by PCR with primers: 5′-GCGGTGAGGACATGATACCTG-3’ and 5′-GGCTGATGGGTGAGTAGAAC-3’, then cloned into pGEM-T vector (Promega). According to the manufacturer’s instructions, *in vitro* transcription of cRNA probes was performed with T7 or SP6 RNA polymerase (Roche) using the template plasmid

iNeurosci Accepted Manuscript

linearized with NcoI and NdeI restriction enzyme sites and RNA DIG labeling mix (Roche). For ISH and IHC, P0 and P2 pups were anesthetized on ice and perfused with ice-cooled 4% paraformaldehyde (PFA) in PBS. Brains were dissected out, fixed in 4% PFA in PBS at 4°C overnight, cryoprotected in 30% sucrose in PBS at 4°C overnight, and then embedded in Tissue-Tek® O.C.T. compound (Sakura Finetek USA, Inc.). Cryostat sections (16 µm-thick) were thaw-mounted onto SuperFrost® glass slides (Matsunami Glass Ind., Ltd) and stored at −80°C until use. ISH was conducted as described previously (Yagi et al., 2016). Briefly, cryostat sections (16 µm-thick) were dried immediately with a hair dryer for at least 1 h and fixed in 4% PFA in PBS for 10 min at room temperature (RT). The sections were then incubated in 0.2 M HCl for 10 min, followed by permeabilization with Proteinase K (7.9 µg/mL; Roche) digestion for 10 min at 37°C. Then the sections were treated with acetic anhydride in 0.1 M triethanolamine for 10 min. For each step, the slides were rinsed with PBS. Finally, the sections were transferred to 5 × saline sodium citrate (SSC) for 10 min or longer. Hybridization was carried out with the generated probes in the hybridization buffer (50% formamide, 5 × SSC, 200 µg/mL yeast tRNA) for at least 16 h at 55°C. The following day, stringency washes were performed in the following steps: 5 × SSC, 20 min at RT; 2 × SSC, 20 min at 65°C; two washes with 0.2 × SSC, 20 min at 65°C and lastly, the slides were transferred to PBS at RT. Detection of specific hybridization was performed using anti-digoxigenin coupled with alkaline phosphatase (anti-DIG-AP) (Roche) at 4°C overnight, and subsequently visualized using nitro blue tetrazolium chloride/5-bromo-4-chloro-3-indolyl-phosphate (NBT/BCIP) at RT. Sense probes were used as negative controls and no signals were observed with the sense probes. In the case of double immunolabeling, ISH treated sections were washed in PBS and then proceeded to IHC.

IHC against Ctip2 was conducted as described previously (Taniguchi et al., 2022). After being air-dried for 1 h at RT, the sections were treated in PBS. Sections were then blocked for 1 h with 5% BSA, 0.1% Triton X-100 in PBS, and then immunostained overnight at 4°C with rat anti-Ctip2 antibody (Abcam, 1:500) followed by incubation with donkey anti-rat IgG H&L conjugated with biotin (Abcam, 1:1000) for 4–6 h at 4°C. For detection of biotinylated secondary antibody binding sites, sections were visualized using a Vectastain Elite ABC kit (Vector Laboratories Inc.) according to the manufacturer's instructions. After amplification with avidin-biotin complex from the Vectastain Elite ABC kit, reaction products were visualized with 0.05 M Tris-HCl buffer (TBS; pH 7.6) containing 0.05% diaminobenzidine tetrahydrochloride (DAB)

JNeurosci Accepted Manuscript

and 0.01% hydrogen peroxide. Images were captured using an upright microscope (model BX-50, Olympus).

IHC against VGluT2 for cortical area identification was conducted as described previously (Potts et al., 2020). In brief, the free-floating sections (50 μm-thick) were washed three times with PBS for 5 min at RT. Then sections were blocked for 1 h at RT with 5% normal donkey serum, 0.1% Triton X-100 in PBS. Next, sections were immunostained overnight at 4°C with rabbit anti-VGLUT2 antibody (1:500) (Synaptic Systems) then washed three times with PBS. Then sections were incubated with secondary antibody Donkey Anti-Rabbit IgG H&L conjugated with Alexa Fluor® 488 (Abcam, 1:200) for 2 h at RT, stained for 10 min with DAPI in PBS, and washed three times in PBS before being mounted using the fluorescence mounting medium Fluoromount (Diagnostic BioSystems, Inc.). Images were captured using a confocal microscope (BZ-X800L, Keyence).

IHC against PTPRO for in vivo knockdown validation was conducted as described previously (Potts et al., 2020). In brief, the free-floating sections (30 μm-thick) were washed three times with PBS for 5 min at RT. Then sections were blocked for 1 h at RT with 5% normal donkey serum, 0.1% Triton X-100 in PBS. Next, sections were immunostained for 48 h at 4°C with rabbit anti-PTPRO antibody (1:250; Sigma-Aldrich) then washed three times with PBS. Then sections were incubated with secondary antibody Alexa Fluor™ 488 donkey anti-rabbit IgG (H+L) (1:200; Thermo Scientific) for 2 h at RT, stained for 10 min with DAPI in PBS, and washed three times in PBS before being mounted using the fluorescence mounting medium Fluoromount (Diagnostic BioSystems, Inc.). Images were captured using a confocal laser scanning microscope (FV3000, Olympus).

***In utero* electroporation (IUE)**

IUE was conducted at E12.5 as described previously (Nagano et al., 2002; Zhu et al., 2009; Iguchi et al., 2021). Briefly, pregnant ICR mice were deeply anesthetized by intraperitoneal injection of a combination anesthetic (MMB: 0.3 mg/kg medetomidine, 4.0 mg/kg midazolam, and 5.0 mg/kg butorphanol) before the experiments. Approximately 1–2 μL of plasmid DNA (2.0–3.5 μg/μL in total) together with Fast Green (final concentration, 0.01%) was injected into the lateral ventricle of the embryos with a glass micropipette (catalog #GD-1.5, Narishige). The ratios of each plasmid were: pCAGGS-tdTomato (Shaner et al., 2004):

JNeurosci Accepted Manuscript

pLKO.1-shRNA vector = 0.5:0.3; pCAGGS-tdTomato: pLKO.1-shRNA vector: pCAGGS-PTPRO-FLAG = 0.5:0.3:0.1; pCAGGS-tdTomato: pLKO.1-shRNA vector: pCAGGS-PTPRO^{DA}-FLAG or pCAGGS-PTPRO^{NTD}-FLAG = 0.5:0.3:0.1; pCMV-Cre: pCA-mTmG (Muzumdar et al., 2007): pCAG-DIO-iCre (Oka et al., 2021) = 0.1:2000:20; pCAGGS-tdTomato: pCAGGS-PTPRO-FLAG or pCAGGS-PTPRO^{DA}-FLAG or pCAGGS-PTPRO^{NTD}-FLAG = 1:3; pCAGGS-tdTomato: pCAGGS-TrkB-v5 = 1:3. pLKO.1-sh*Scramble* (Iguchi et al., 2021) was used as a control. After soaking the uterine horn with phosphate-buffered saline (PBS), the head of the embryo was pinched with a forceps-type electrode (CUY650P3, NEPAGENE), and five cycles of square electric pulses (34 V, 50 ms duration with 950 ms intervals) were delivered using an electroporator (CUY21EDIT, NEPAGENE). The uterine horns were returned to the abdominal cavity, and the incision was sutured. After recovery, the embryos were allowed to continue normal development.

DiI injection and tissue preparation

To make the map for DiI (Thermo Fisher Scientific) labeling, P2 pups were anesthetized on ice and perfused with ice-cooled 4% PFA in PBS. Brains were dissected out and fixed in 4% PFA in PBS at 4°C overnight. Ten percent DiI solution in dimethylformamide was spotted on the surface of the cortex in the form of a dot and arranged in two rows. Then brains were placed into agar solution (2.5% agar), cut into 50-μm-thick coronal sections using a microslicer (model DTK-1000, Dosaka EM), and sections before IHC were treated in PBS at 4°C. Images with DiI were captured using a research slide scanner (Slideview VS200, Olympus).

To analyze axon collaterals, P1, P2 and P4 pups were anesthetized on ice and perfused with ice-cooled 4% PFA in PBS. Brains were dissected out, fixed in 4% PFA in PBS at 4°C overnight, placed into agar solution (2.5% agar), and cut parasagittally into 100-μm-thick sections using a microslicer (model DTK-1000, Dosaka EM). Sections were made at an angle that included the entire axon and collaterals in the pons. Images were captured using a fluorescence microscope (AxioObserver A1, Carl Zeiss).

To analyze axon collateral branches, P2 pups were anesthetized on ice and perfused with ice-cooled 4% PFA in PBS. Brains were dissected out, fixed in 4% PFA in PBS at 4°C overnight, placed into agar solution (2.5% agar), and cut parasagittally into 500-μm-thick sections. Optical clearing was performed with the SeeDB2 method (Ke et al., 2016) with modifications. 500-μm-thick sections were immersed in iohexol containing 0.5% Triton X-100 and DAPI (1:1000) and incubated at 25°C overnight. For imaging, cleared

JNeurosci Accepted Manuscript

sections were mounted in the final clearing solution between two coverslips with silicone rubber spacers. Cleared brains were imaged with a confocal laser scanning microscope (LSM 880 with Airyscan, Zeiss).

Axon collateral branch tracing

Tracing was performed as previously described (Oka et al., 2021). In brief, three-dimensional reconstruction of confocal images and tracing of axons, collaterals and branches were performed using Neurolucida® software (version 11, MBF Bioscience). Axons, collaterals, and branches in the pons were traced by manually registering the EGFP signal on each focal plane starting from the beginning to the end of the signal.

Cell culture and transfection

HEK293T cells [293T (ATCC CRL-3216)] (American Type Culture Collection) were cultured as described previously (Nguyen et al., 2022). In brief, cells were cultured in 1× Dulbecco's modified Eagle's medium (DMEM) (Nacalai Tesque) with 10% fetal bovine serum (Sigma-Aldrich), 100 U/mL penicillin (Meiji Seika Pharma Co., Ltd), and 100 μg/mL streptomycin (Sigma-Aldrich) at 37°C in a humidified incubator with 5% CO_2. For cell line maintenance, HEK293T cells were cultured in 10 cm plastic dishes (Thermo Fisher Scientific). For analysis of the membrane localization of PTPRO and its variants, HEK293T cells were seeded in removable four-well chambered glass slides (Matsunami Glass Ind., Ltd) coated with 0.0033% poly-L-lysine solution diluted from poly-L-lysine powder (Sigma-Aldrich). Cells were co-transfected with the plasma membrane marker Lyn11-EGFP (Nguyen et al., 2022) and one of the following FLAG-tagged expression constructs: pCAGGS-PTPRO-FLAG, pCAGGS-PTPRO^{DA}-FLAG, or pCAGGS-PTPRO^{NTD}-FLAG. For cell-surface detection of PTPRO^{NTD} under non-permeabilizing conditions, cells were separately transfected with pEB-PPTsp-V5-PTPRO^{NTD}. Transfections were performed using linear polyethylenimine (PEI; Polysciences, Inc.). The medium was replaced 3 h after transfection to minimize PEI-induced cytotoxicity.

For analysis of knockdown efficiency, HEK293T cells were seeded in 24-well plates and co-transfected with pCAGGS-PTPRO-FLAG or pCAGGS-TrkB-V5 together with the corresponding shRNA expression

JNeurosci Accepted Manuscript

vectors using PEI. The medium was replaced 3 h after transfection to minimize PEI-induced cytotoxicity.

Primary Cortical Neuron Culture

Cortical neurons were isolated from E16 ICR mouse embryos. Briefly, four-well chambered glass slides (Matsunami Glass Ind., Ltd) were coated with 1× branched polyethylenimine (PEI) diluted in sterile $Na_2B_4O_7$ buffer (pH 8.4). Embryonic cortices were dissected in ice-cold PBS, digested with papain solution for 20 min at 37°C. Tissues were mechanically triturated, filtered through a 40-μm strainer, and centrifuged at 1,000 x *g* for 20 min. Cells were seeded at a density of 1 x 10^5 cells/well in plating medium (50% Neurobasal, 25% horse serum, 25% HBSS). After 3 h, the medium was replaced with maintenance medium (Neurobasal supplemented with B-27 Plus, 0.5 mM GlutaMAX, and 0.1% penicillin-streptomycin). Neurons were maintained at 37°C with 5% CO_2.

Immunocytochemistry

To analyze the membrane localization of PTPRO, $PTPRO^{DA}$, and $PTPRO^{NTD}$, HEK293T cells were fixed 48 h after transfection in 4% PFA in PBS for 15 min and then washed three times with PBS. Cells expressing PTPRO-FLAG or $PTPRO^{DA}$-FLAG or $PTPRO^{NTD}$-FLAG and Lyn11-EGFP were permeabilized with 0.25% Triton X-100 in PBS for 5 min and then washed three times with PBS. Cells expressing V5-$PTPRO^{NTD}$ were not permeabilized. Cells were blocked with 10% normal donkey serum in PBS for 1 h at RT. Next, staining with anti-FLAG (Santa Cruz Bio, Inc.) or anti-V5 antibody (Invitrogen/Thermo Scientific) (1:500 dilution in 2% normal donkey serum in PBS, respectively) was performed for 1 h at RT then washed three times with PBS. Then, the cells were incubated with secondary antibody Alexa Fluor™ 568 donkey anti-Goat IgG (H+L) (Invitrogen/Thermo Scientific) or Donkey Anti-Mouse IgG H&L (Alexa Fluor® 488) (Abcam) (1:200 dilution in 2% normal donkey serum in PBS, respectively) for 30 min at RT, washed twice with PBS, stained for 5 min with DAPI in PBS, and washed twice more in PBS before being mounted using the fluorescence mounting medium Fluoromount (Diagnostic BioSystems, Inc.). Cells were imaged with a confocal laser scanning microscope (LSM 880 with Airyscan, Zeiss).

Neurons were fixed at DIV 7 with 4% PFA in PBS for 10 min at RT, then washed three times with PBS. Cells were permeabilized with 0.25% Triton X-100 in PBS for 5 min. Blocking was performed with 5%

JNeurosci Accepted Manuscript

normal donkey serum in PBS for 1 h. The cells were incubated with goat anti-TrkB (1:500; R&D Systems), rabbit anti-PTPRO (1:500; Sigma-Aldrich), and chicken anti-MAP2 (1:1000; Synaptic Systems) in 5% normal donkey serum overnight at 4°C. After three PBS washes, cells were incubated with secondary antibodies including Alexa Fluor™ 568 donkey anti-goat IgG (H+L) (Invitrogen/Thermo Scientific) and Alexa Fluor™ 488 donkey anti-rabbit IgG (H+L) (Thermo Scientific), and Alexa Fluor® 647-conjugated AffiniPure® Donkey anti-chicken IgG (H+L) (Jackson ImmunoResearch) (1:200 dilution in PBS, respectively) for 1 h at RT. Nuclei were stained with DAPI for 5 min. Coverslips were mounted using Fluoromount and imaged with a confocal laser scanning microscope (LSM 880 with Airyscan, Zeiss).

Western blotting

HEK293T cells subcultured in 24- or 6-well plates were transfected with pCAGGS-PTPRO-FLAG and shRNA constructs, or pCAGGS-PTPRO-FLAG or pCAGGS-PTPRO^{DA}-FLAG or pCAGGS-PTPRO^{NTD}-FLAG and pCAGGS-TrkB-V5. The total amount of DNA was 500 ng/well or 4 μg/well. The ratio of the shRNA plasmid to the PTPRO-FLAG or TrkB-V5 expression plasmid was 3:1. The culture media was renewed 3 h after transfection, and cells were cultured for 48 h post transfection. After 48 h, cells were washed three times with ice-cold PBS, then collected and centrifuged at 1,000 x *g* for 5 min at 4°C. Cells were lysed for 10 min on ice in lysis buffer containing 50 mM Tris-HCl (pH 7.5), 150 mM NaCl, 1% NP-40, and protease inhibitor cocktail (Nacalai Tesque, Inc.). The lysates were then centrifuged at 15,000 rpm for 10 min at 4°C. The supernatants were collected, mixed with sample buffer, and heated at 95°C for 5 min. The proteins were separated by SDS-PAGE and transferred to polyvinylidene difluoride membrane (EMD Millipore). The membranes were blocked with 5% skim milk in TBST (0.05% Tween-20, 50 mM Tris-HCl, 138 mM NaCl, 2.7 mM KCl) or 5% BSA in TBST at RT for at least 1 h, then incubated with HRP-conjugated mouse anti-DDDDK (Medical & Biological Laboratories Co., Ltd.), or HRP-conjugated rabbit anti-β-actin (Medical & Biological Laboratories Co., Ltd.), or HRP-conjugated mouse anti-V5 (Medical & Biological Laboratories Co., Ltd.) (1:2000 dilution in 5% skim milk in TBST, respectively), or mouse anti-phosphotyrosine (clone 4G10, Millipore, 1:1000 dilution in 5% BSA in TBST) and HRP-conjugated anti-mouse IgG (Cell Signaling Technology, 1:5000 dilution in 5% BSA in TBST). Antibodies were washed off by shaking membranes in TBST three times for 15 min each. Detection was done using Immobilon

JNeurosci Accepted Manuscript

Crescendo Western HRP substrate (EMD Millipore). Images were captured with LAS-3000 mini (FUJIFILM), and the band intensity was analyzed using ImageJ software (National Institutes of Health).

Postnatal Drug Administration

ICR mouse pups electroporated at E12.5 were randomly assigned to treatment groups. From P0 to P2, pups received a once-daily intragastric injection of BKM120 (3 mg/kg in peanut oil) using a procedure adapted from a previous study (Pitulescu et al., 2010). Briefly, the pups were temporarily separated from the dam and maintained under a warming lamp with the ventral abdomen exposed. The milk-filled stomach was visualized through the translucent abdominal wall, and a needle was carefully inserted percutaneously into the stomach lumen at a shallow angle (10–15°). The solution was administered slowly to minimize reflux, and successful intragastric delivery was confirmed by visible distension of the stomach. Immediately after each injection, the pups were returned to the dam to minimize separation stress. Following the final injection at P2, tissues were collected within 2 h.

Quantification and statistical analysis

To analyze the distribution of axon collaterals in the pons, images were first rotated to align the pons and the corticospinal axonal shaft to a consistent orientation. The region of the pons underneath the corticospinal axonal shaft, extending from the lower edge of the axonal shaft to the ventral boundary of the pons, was evenly divided into 10 or 5 bins along the vertical axis (Figs. 2*C* and 3*G*). The height of each bin therefore corresponded to 10% or 20%, respectively, of this distance and was normalized to the size of the analyzed pontine region in each sample. The ratio of the fluorescence intensity of each bin to the fluorescence intensity of the axon main shaft was analyzed using ImageJ (NIH).

To quantify the branching architecture of corticopontine axon collaterals in the pons, individual axons and their collateral arbors were traced. For each axon, the total number of collaterals was counted, and for each collateral, the total number of branches was determined. Each collateral arising from the main axonal shaft was designated as order 0. Branches arising from the first bifurcation were classified as primary branches, and the branch order was increased by one at each subsequent bifurcation. Each branch was also assigned to the corresponding dorsoventral bin according to its location within the pons. Branch counts, branch-order distributions, and dorsoventral distributions were calculated using Microsoft Excel (Microsoft 365). For each

JNeurosci Accepted Manuscript

mouse, the collateral complexity index was calculated by dividing the branch-order-weighted sum of all branches across the analyzed collaterals by the total number of collaterals analyzed, as described previously (Marshak et al., 2007). Each mouse yielded one collateral complexity index value and served as the statistical unit.

Statistical analyses were performed using GraphPad Prism 8 (GraphPad Software, San Diego, CA, USA). Data are presented as the mean ± SEM. All statistical tests were two-sided, and $p < 0.05$ was considered statistically significant. Data distributions were assessed using the Shapiro–Wilk test, and homogeneity of variance was assessed using the Brown–Forsythe test. For comparisons between two groups, Welch's unpaired *t* test was used for normally distributed data, whereas the Mann–Whitney *U* test was used for data that did not meet the assumption of normality. For comparisons among three or more groups, ordinary one-way ANOVA followed by Tukey's multiple-comparisons test was used when the assumptions of normality and homogeneity of variance were met. Welch's one-way ANOVA followed by Tamhane's T2 multiple-comparisons test was used for normally distributed data with unequal variances, whereas the Kruskal–Wallis test followed by Dunn's multiple-comparisons test was used for data that did not meet the assumption of normality. For analysis of TrkB phosphorylation in the matched immunoblot experiments, one-way repeated-measures ANOVA with the Geisser–Greenhouse correction followed by Tukey's multiple-comparisons test was used. Frequency distributions were compared using the Kolmogorov–Smirnov test. The statistical test and sample size used for each experiment are specified in the corresponding Results section or figure legend.

JNeurosci Accepted Manuscript

Results

PTPRO was identified as a candidate regulator of corticospinal collateral development

To identify receptor-type protein tyrosine phosphatases (RPTPs) that may regulate corticospinal collateral development, we first analyzed publicly available transcriptomic datasets of corticospinal projection neurons. From the RPTP family, several genes (*Ptprf*, *Ptprk*, *Ptpro*, *Ptprs*, *Ptprt*, *Ptprz1*) were found to be highly expressed in these neurons at the stage of collateral formation (Fig. S1*A*, *B* and Table S1). We next performed an in vivo knockdown screen using *in utero* electroporation (IUE) to test their potential roles in corticospinal collateral development toward the pontine nuclei. Among the candidate genes examined, knockdown of *Ptpro* produced a clear phenotype in corticospinal collateral development, leading us to focus on PTPRO in subsequent analyses (Fig. S1*C*).

Ptpro was expressed in layer 5 neurons of the developing cerebral cortex

Ptpro has been reported to be expressed in upper-layer cortical neurons of the early postnatal cortex (Beltran et al., 2003), whereas its expression in deeper layers remains uncharacterized. To systematically characterize its regional and laminar expression pattern, we performed *in situ* hybridization (ISH) on postnatal day 0 (P0) mouse brains. At the regional level, we observed *Ptpro* expression in the somatosensory and motor cortices, as well as in the visual and auditory cortices at P0, with comparatively lower expression in the latter two regions (Fig. 1*A*). At the laminar level, we found *Ptpro* concentrated in L2/3, L4, and L5 cortical neurons of the frontal and parietal regions, but only faintly expressed in L5 cortical neurons of the occipital regions (Figs. 1*B*, *C* and S1*D*). To confirm *Ptpro* expression in L5 cortical neurons, we combined immunohistochemistry (IHC) against the L5 marker Ctip2 (Arlotta et al., 2005) with ISH analyses. We found that *Ptpro* and Ctip2 were co-expressed in most L5 cortical neurons of the frontal and parietal regions (Figs. 1*B*, *C* and S1*D*).

To assess *Ptpro* expression in developing L5 cortical neurons, we performed RT-PCR analysis on *Fezf2*-positive L5 neurons collected at key developmental stages (embryonic day (E) 13, E15, E17, and P0) as *Fezf2* is a key transcriptional regulator of corticospinal and other subcerebral projection neuron identity (Molyneaux et al., 2005; Eckler et al., 2014). Previous studies (Beltran et al., 2003) reported peak *Ptpro* expression in the CNS between E16 and P3, with two identified splice variants: a long-form containing 28

JNeurosci Accepted Manuscript

amino acids in the juxtamembrane domain and a short-form lacking this insertion. Using variant-specific primers in *Fezf2*-expressing L5 neurons, we found the long-form *Ptpro* transcript was consistently expressed from E13 through P0, while the short-form showed weaker but detectable expression specifically at P0 (Fig. S1*E*). Consistent with these findings, supplementary data from an independent transcriptomic study detected *Ptpro* in corticospinal neurons identified by spinal retrograde labeling and purified by FACS during early postnatal development (Sahni et al., 2021). Together, our ISH/IHC and *Fezf2*-positive neuron analyses, combined with these projection-defined transcriptomic data, support *Ptpro* expression in developing corticospinal neurons.

Knockdown of *Ptpro* resulted in increased corticospinal collateral signal in the pons

To examine whether PTPRO is involved in corticospinal collateral development, we knocked down *Ptpro* in neurons of the cerebral cortex and observed phenotypes at P2 (Fig. 2*A*). Five *Ptpro*-targeting shRNAs were first evaluated in HEK293T cells (Fig. S2*A*). We transfected the knockdown plasmid for *Ptpro* together with the tdTomato expression plasmid by IUE at E12.5 to suppress PTPRO expression in the corticospinal neurons at different cortices (Fig. 2*B*). To validate PTPRO knockdown in vivo, we performed IHC for PTPRO on cortical sections following IUE. PTPRO immunoreactivity in tdTomato-positive neurons was markedly reduced following *Ptpro* knockdown compared with the sh*Scramble* control (Fig. S2*B*). Quantification of PTPRO fluorescence intensity within tdTomato-positive neuronal regions confirmed a significant reduction in the sh*Ptpro* group [Welch's *t* test; $t(2.865) = 6.342$, $p = 0.0091$] (Fig. S2*C*), demonstrating effective PTPRO knockdown in vivo. To precisely localize cortical areas for IUE-mediated knockdown analysis, we first established anatomical landmarks by injecting DiI dye at standardized coordinates corresponding to motor, somatosensory, and auditory cortices (Fig. S2*D*). Cortical area identity was further verified by VGLUT2 expression patterns, which show distinct regional distributions across these functional domains (Fig. S2*E*). Building upon established molecular markers of cortical arealization (Suzuki et al., 1997), we generated a comprehensive P2 cortical map based on cadherin-6, -8, and -11 expression patterns (Fig. S2*F*). This molecular map served as the basis for categorizing IUE experimental results, allowing precise areal assignment of knockdown phenotypes. To quantify the axon collateral signal in the pons, we divided regions of the pons underneath the corticospinal axonal shaft into 10 bins along the dorsoventral axis and

JNeurosci Accepted Manuscript

453 measured the fluorescence intensity in each bin as collateral distribution along the dorsoventral axis (Fig.
454 2*C*). The fluorescence intensity in the pons was increased in bins 1-5 of motor cortex *Ptpro*-knockdown
455 corticospinal neurons relative to controls [Welch's *t* test; bin 1, $t(5.418) = 4.415$, $p = 0.0057$; bin 2, $t(5.519)$
456 $= 3.455$, $p = 0.0155$; bin 3, $t(5.843) = 3.537$, $p = 0.0128$; bin 4, $t(5.654) = 3.259$, $p = 0.0188$; bin 5, $t(5.422)$
457 $= 3.129$, $p = 0.0233$] (Fig. 2*D*, *E)*. In the somatosensory cortex, *Ptpro*-knockdown corticospinal neurons
458 showed a significant increase in fluorescence intensity in bins 1-6 compared with controls [Welch's *t* test;
459 bin 1, $t(7.772) = 5.465$, $p = 0.0007$; bin 2, $t(7.339) = 6.975$, $p = 0.0002$; bin 3, $t(9.932) = 6.606$, $p < 0.0001$;
460 bin 4, $t(9.997) = 5.041$, $p = 0.0005$; bin 5, $t(9.816) = 3.857$, $p = 0.0033$; bin 6, $t(10.00) = 2.736$, $p = 0.0210$]
461 (Fig. 2*F*, *G*). However, the fluorescence intensity was not increased in auditory cortex *Ptpro*-knockdown
462 corticospinal neurons [Welch's *t* test; all $p > 0.05$] (Fig. S2*G*, *H*). The increase in fluorescence intensity was
463 fully rescued by the co-transfection of the shRNA-resistant PTPRO expression vector together with the
464 shRNA vector [one-way ANOVA followed by Tukey's multiple-comparisons test; sh*Ptpro* + Mock vs sh*Ptpro*
465 + *Ptpro*-res, bin 1, $F(2, 15) = 14.65$, ANOVA $p = 0.0003$, Tukey-adjusted $p = 0.0007$; bin 2, $F(2, 15) = 19.18$,
466 ANOVA $p < 0.0001$, Tukey-adjusted $p = 0.0003$; bin 3, $F(2, 15) = 10.39$, ANOVA $p = 0.0015$, Tukey-adjusted
467 $p = 0.0042$; bin 4, $F(2, 15) = 7.718$, ANOVA $p = 0.0050$, Tukey-adjusted $p = 0.0242$] (Fig. 2*H*, *I*). These
468 results indicate that *Ptpro* knockdown increases corticospinal collateral signal in the motor and
469 somatosensory cortical projections to the pons.

470 We also examined the corticospinal collateral signal at P1 to determine whether the increase following
471 *Ptpro* knockdown was detectable at an earlier developmental stage. The fluorescence intensity was
472 increased in bins 1, 2, and 4 in the motor cortex *Ptpro*-knockdown corticospinal neurons compared with
473 controls [Welch's *t* test; bin 1, $t(3.477) = 7.007$, $p = 0.0036$; bin 2, $t(3.149) = 3.164$, $p = 0.0474$; bin 4, $t(3.822)$
474 $= 4.155$, $p = 0.0156$] and increased in bin 1 to bin 8 in the somatosensory cortex *Ptpro*-knockdown
475 corticospinal neurons compared with controls [Welch's *t* test; bin 1, $t(6.117) = 8.022$, $p = 0.0002$; bin 2,
476 $t(8.442) = 7.422$, $p < 0.0001$; bin 3, $t(9.673) = 6.879$, $p < 0.0001$; bin 4, $t(10.00) = 7.336$, $p < 0.0001$; bin 5,
477 $t(7.166) = 4.498$, $p = 0.0026$; bin 6, $t(9.752) = 5.321$, $p = 0.0004$; bin 7, $t(9.679) = 3.511$, $p = 0.0059$; bin 8,
478 $t(9.916) = 2.506$, $p = 0.0313$] (Fig. S3*A*–*D*). No differences were observed in the auditory cortex [Welch's *t*
479 test; all $p > 0.05$] (Fig. S3*E*, *F*). The increase in fluorescence intensity was rescued by co-transfection of
480 shRNA-resistant PTPRO expression vector together with the shRNA vector [one-way ANOVA followed by

JNeurosci Accepted Manuscript

Tukey's multiple-comparisons test; sh*Ptpro* + Mock vs sh*Ptpro* + *Ptpro*-res, bin 1, $F(2, 15) = 26.49$, ANOVA $p < 0.0001$, Tukey-adjusted $p < 0.0001$; bin 2, $F(2, 15) = 9.111$, ANOVA $p = 0.0026$, Tukey-adjusted $p = 0.0036$; bin 3, $F(2, 15) = 11.61$, ANOVA $p = 0.0009$, Tukey-adjusted $p = 0.0012$; bin 4, $F(2, 15) = 5.314$, ANOVA $p = 0.0180$, Tukey-adjusted $p = 0.0330$] (Fig. S3*G*, *H*). These results indicate that suppression of *Ptpro* expression increases corticospinal collateral signal as early as P1.

We further examined the corticospinal collateral signal at P4 to determine whether the increase observed following *Ptpro* knockdown persisted at a later developmental stage. Because the somatosensory cortex showed a prominent increase in collateral signal at both P1 and P2, we focused the P4 analysis on corticospinal neurons originating from this cortical area. The fluorescence intensity was increased in the somatosensory cortex *Ptpro*-knockdown corticospinal neurons compared with controls [Welch's *t* test; bin 1, $t(5.863) = 12.95$, $p < 0.0001$; bin 2, $t(9.503) = 11.00$, $p < 0.0001$; bin 3, $t(9.985) = 7.427$, $p < 0.0001$; bin 4, $t(9.984) = 6.819$, $p < 0.0001$; bin 5, $t(8.850) = 5.659$, $p = 0.0003$; bin 6, $t(10.00) = 3.158$, $p = 0.0102$; bin 7, $t(9.586) = 2.592$, $p = 0.0277$; bin 8, $t(9.855) = 3.583$, $p = 0.0051$; bin 9, $t(7.009) = 2.820$, $p = 0.0257$] (Fig. S3*I*, *J*). Together with the findings at P1 and P2, these results indicate that suppression of *Ptpro* expression increases corticospinal collateral signal from P1 through P4.

Knockdown of *Ptpro* resulted in the enhancement of axon collateral arborization in the pons

PTPRO inhibits trigeminal axon growth and branching (Gatto et al., 2013). This raises the possibility that the increase in fluorescence intensity in *Ptpro*-knockdown neurons in the pons was caused by the increase in collateral branch numbers. To assess this hypothesis, we quantitatively analyzed axon collateral arborization within the pons using sparse labeling of individual corticospinal neurons (Oka et al., 2021). We used Cre-dependent Cre expression vector pCAGGS-DIO-iCre, which can improve the recombination efficiency and lead to higher expression of Cre-dependent reporter protein, together with Cre-dependent reporter pCA-mTmG (Muzumdar et al., 2007), in which the expressed fluorescent reporter was switched from membrane-bound tdTomato to membrane-bound EGFP upon recombination (Figs. 3*A* and S4*A*). *Ptpro*-knockdown corticospinal neurons were sparsely labeled using IUE, with pCMV-Cre, pCA-mTmG, pCAGGS-DIO-iCre and sh*Ptpro* at E12.5 (Figs. 3*A* and S4*A*). Brain samples were optically cleared using the SeeDB2 method (Ke et al., 2016) and analyzed by confocal imaging of the pons (Fig. 3*B*). After tracing

JNeurosci Accepted Manuscript

the EGFP signal of the axons, collaterals, and branches in the pons, we analyzed how axon collateral branches formed in the pons. The motor and somatosensory cortex *Ptpro*-knockdown collaterals showed more extensive branching, while control collaterals had few branches in the pons (Figs. 3*C* and S4*E*). However, the number of auditory cortex *Ptpro*-knockdown collateral branches was not changed (Fig. S4*K*). This suggested that *Ptpro* knockdown resulted in the promotion of the formation of collateral arbors. We further characterized collateral morphology in several ways. The total branch number of each axon collateral was significantly increased in *Ptpro*-knockdown collaterals compared with control collaterals from the somatosensory and motor cortex, but not in the auditory cortex [Welch's *t* test; somatosensory cortex, $t(9.086) = 4.157$, $p = 0.0024$; motor cortex, $t(2.286) = 4.497$, $p = 0.0357$] (Fig. S4*C*, *G*, *M*). However, the number of collaterals per axon was not significantly different between *Ptpro*-knockdown and control groups across all cortical regions examined (Fig. S4*B*, *F*, *L*). Frequency distribution analysis of the total number of collateral branches per axon revealed a significant rightward shift in *Ptpro*-knockdown axons toward more highly branched arbors [Kolmogorov-Smirnov test, $D = 0.4263$, $p < 0.0001$] (Fig. S4*D*). To classify collateral morphology, axon collaterals and their branches were categorized into six orders based on their branching hierarchy from the main axonal shaft (Fig. 3*D*). The numbers of primary and secondary branches were significantly higher in *Ptpro*-knockdown collaterals than in control collaterals in both the somatosensory and motor cortices. The number of tertiary branches was also significantly increased in the somatosensory cortex, whereas no significant differences were observed in the auditory cortex [Welch's *t* test; somatosensory cortex, primary, $t(11.21) = 4.320$, $p = 0.0012$; secondary, $t(7.918) = 3.351$, $p = 0.0102$; tertiary, $t(7.820) = 3.109$, $p = 0.0149$; motor cortex, primary, $t(3.259) = 4.263$, $p = 0.0200$; secondary, $t(3.091) = 4.525$, $p = 0.0189$; auditory: $p > 0.05$] (Figs. 3*E*, S4*I*, *O*). Collateral complexity index, which accounts for the number of branches of different orders (Marshak et al., 2007), was significantly higher in *Ptpro*-knockdown collaterals than in control collaterals in the somatosensory and motor cortices, but not in auditory cortex [Welch's *t* test; somatosensory cortex, $t(8.085) = 3.732$, $p = 0.0057$; motor cortex, $t(3.386) = 7.530$, $p = 0.0032$; auditory cortex: $p > 0.05$], suggesting that collateral branches were composed mainly of higher-order branches (Figs. 3*F*, S4*H*, *N*). When the region of the pons underneath the corticospinal axonal shaft was divided into 5 bins along the dorsoventral axis (Fig. 3*G*), collateral branch numbers were significantly higher in bins 1 and 2 in *Ptpro*-knockdown collaterals than in control collaterals in both the

JNeurosci Accepted Manuscript

somatosensory and motor cortices. An additional increase in bin 3 was observed in the somatosensory cortex, whereas no significant differences were detected in the auditory cortex [Welch's *t* test; somatosensory cortex, bin 1, $t(10.41) = 4.632$, $p = 0.0008$; bin 2, $t(8.227) = 4.366$, $p = 0.0022$; bin 3, $t(11.43) = 2.343$, $p = 0.0382$; motor cortex, bin 1, $t(3.918) = 6.422$, $p = 0.0032$; bin 2, $t(5.909) = 6.607$, $p = 0.0006$; auditory cortex: $p > 0.05$] (Figs. 3*H*, S4*J*, *P*). These results suggest that the suppression of *Ptpro* expression in the corticospinal neurons enhanced the axon collateral arborization in the pons.

PTPRO phosphatase activity was required to suppress axon collateral arborization in the pons

PTPRO contains eight extracellular fibronectin type III-like domains and one intracellular phosphatase domain (Tautz et al., 2013). Next, we asked which domain of PTPRO was essential for axon collateral arborization. To address this question, we constructed a substrate-trapping mutant in which the key residue of the intracellular phosphatase domain was substituted (PTPRO^{DA}-FLAG, D1112A) (Flint et al., 1997; Motiwala et al., 2010; Hsu et al., 2013), and generated N-terminal deletion constructs of PTPRO (PTPRO^{NTD}-FLAG and V5-PTPRO^{NTD}) (Jiang et al., 2017) (Fig. 4*A*). We first examined the membrane localization of PTPRO, PTPRO^{DA}, and PTPRO^{NTD} by immunofluorescence in HEK293T cells co-transfected with each FLAG-tagged construct and the plasma membrane marker Lyn11-EGFP (Nguyen et al., 2022). All three variants colocalized with Lyn11-EGFP at the plasma membrane (Fig. S5*A*–*C*), confirming correct membrane targeting regardless of extracellular domain deletion or phosphatase inactivation. We then tested whether these variants could rescue the axon arborization defect caused by *Ptpro* knockdown. Co-transfection of the *Ptpro* knockdown plasmid with the shRNA-resistant extracellular-domain-deletion construct PTPRO^{NTD} rescued the phenotype, whereas co-transfection with the phosphatase-dead mutant PTPRO^{DA} did not [one-way ANOVA followed by Tukey's multiple-comparisons test; *Ptpro*-res vs *Ptpro*^{DA}, bin 1, $F(2, 15) = 8.644$, ANOVA $p = 0.0032$, Tukey-adjusted $p = 0.0162$; bin 2, $F(2, 15) = 8.965$, ANOVA $p = 0.0027$, Tukey-adjusted $p = 0.0072$; bin 3, $F(2, 15) = 7.390$, ANOVA $p = 0.0058$, Tukey-adjusted $p = 0.0192$] (Fig. 4*B*–*D*). These results indicate that PTPRO phosphatase activity, but not its extracellular domain, is required for PTPRO-mediated suppression of axon collateral arborization in the pons.

Overexpression of PTPRO resulted in poor axon collateral arborization in the pons

JNeurosci Accepted Manuscript

Knockdown of *Ptpro* resulted in an increase of axon collateral arborization (Fig. 3). We next examined whether the overexpression of PTPRO resulted in a decrease in axon collateral arborization. We transfected pCAGGS-5MCS-FLAG, pCAGGS-PTPRO-FLAG, pCAGGS-PTPRO^{DA}-FLAG and pCAGGS-PTPRO^{NTD}-FLAG by IUE at E12.5 to overexpress PTPRO in the corticospinal neurons (Fig. 5*A*). We found that the fluorescence intensity decreased from bins 1-4 in the collaterals extended from axons of PTPRO and PTPRO^{NTD} overexpressing corticospinal neurons compared with those from axons of PTPRO^{DA} and control corticospinal neurons [one-way ANOVA followed by Tukey's multiple-comparisons test; Mock vs PTPRO, Mock vs PTPRO^{NTD}; bin 1, $F(3, 20) = 29.57$, ANOVA $p < 0.0001$, Tukey-adjusted $p < 0.0001$, $p < 0.0001$; bin 2, $F(3, 20) = 34.87$, ANOVA $p < 0.0001$, Tukey-adjusted $p < 0.0001$, $p < 0.0001$; bin 3, $F(3, 20) = 14.56$, ANOVA $p < 0.0001$, Tukey-adjusted $p = 0.0014$, $p = 0.0016$; bin 4, $F(3, 20) = 9.064$, ANOVA $p = 0.0005$, Tukey-adjusted $p = 0.0258$, $p = 0.0070$] (Fig. 5*B*). These results suggest that PTPRO overexpression suppresses axon collateral arborization in the pons.

To further validate the effect of PTPRO overexpression on individual neuron collateral arborization, we performed sparse labeling to trace single corticospinal axons and their collaterals (Fig. 5*C*). Consistent with the population-level analysis, the number of collaterals per axon was not significantly different among Mock, PTPRO, PTPRO^{DA} and PTPRO^{NTD} groups (Fig. 5*D*). However, the number of branches per collateral was significantly reduced in PTPRO and PTPRO^{NTD} overexpressing neurons compared with Mock and PTPRO^{DA} controls [one-way ANOVA followed by Tukey's multiple-comparisons test; Mock vs PTPRO, Mock vs PTPRO^{NTD}; $F(3, 20) = 19.41$, ANOVA $p < 0.0001$, Tukey-adjusted $p < 0.0001$, $p < 0.0001$] (Fig. 5*E*). Collateral complexity index was also significantly decreased in PTPRO and PTPRO^{NTD} overexpressing collaterals compared with both control groups, indicating reduced arborization complexity [one-way ANOVA followed by Tukey's multiple-comparisons test; Mock vs PTPRO, Mock vs PTPRO^{NTD}; $F(3, 20) = 20.08$, ANOVA $p < 0.0001$, Tukey-adjusted $p < 0.0001$, $p < 0.0001$] (Fig. 5*F*). Furthermore, numbers of primary and secondary branches were significantly reduced in PTPRO and PTPRO^{NTD} overexpressing neurons compared with Mock and PTPRO^{DA} controls, whereas tertiary, quaternary, and quinary branches showed no significant differences [primary, one-way ANOVA followed by Tukey's multiple-comparisons test; Mock vs PTPRO, Mock vs PTPRO^{NTD}; $F(3, 20) = 18.76$, ANOVA $p < 0.0001$, Tukey-adjusted $p = 0.0002$, $p = 0.0001$; secondary, Kruskal–Wallis test followed by Dunn's multiple-comparisons test; Mock vs PTPRO,

JNeurosci Accepted Manuscript

590 Mock vs PTPRO^{NTD}; $H(3) = 19.21$, Kruskal–Wallis $p = 0.0002$, Dunn-adjusted $p = 0.0022$, $p = 0.0066$] (Fig.
591 5*G*). When collateral branch distribution was analyzed along the dorsoventral axis, branch numbers in bin
592 1 were significantly reduced in PTPRO and PTPRO^{NTD}-overexpressing collaterals compared with Mock
593 controls, whereas neither group differed significantly from Mock controls in bins 2–5 [bin 1, one-way ANOVA
594 followed by Tukey's multiple-comparisons test; Mock vs PTPRO, Mock vs PTPRO^{NTD}; $F(3, 20) = 27.37$,
595 ANOVA $p < 0.0001$, Tukey-adjusted $p < 0.0001$, $p = 0.0005$] (Fig. 5*H*). Taken together, these results confirm
596 that overexpression of PTPRO suppresses axon collateral arborization at the level of individual corticospinal
597 neurons in the pons.

598 **PTPRO suppressed axon collateral arborization through inhibition of TrkB signaling**

599 Gatto et al. (2013) showed that PTPRO inhibits trigeminal axon growth and branching by repressing TrkB
600 and Ret signaling. TrkB is therefore a plausible substrate of PTPRO in collateral arborization. To investigate
601 whether TrkB signaling was involved in axon collateral arborization, we first examined the co-expression of
602 PTPRO with TrkB in cultured cortical neurons by immunofluorescence staining. PTPRO and TrkB were
603 found to co-express in MAP2-positive neurons, and approximately 81.6 ± 8.9% of PTPRO-positive neurons
604 expressed TrkB (Fig. S6*A*, *B*), suggesting that PTPRO and TrkB are co-expressed in the same neuronal
605 population. We then co-transfected TrkB-V5 and PTPRO-FLAG into HEK293T cells to examine their
606 interaction. Co-immunoprecipitation revealed that PTPRO interacted with TrkB, and the presence of wild-
607 type PTPRO markedly reduced TrkB phosphotyrosine intensity, whereas the phosphatase-dead mutant
608 PTPRO^{DA} failed to suppress TrkB phosphorylation [one-way repeated-measures ANOVA with Geisser–
609 Greenhouse correction, $F(2.473, 7.420) = 48.26$, ANOVA $p < 0.0001$, followed by Tukey's multiple-
610 comparisons test; Mock vs WT: Tukey-adjusted $p = 0.0056$; WT vs DA, Tukey-adjusted $p = 0.0280$] (Fig.
611 6*A*, *B*). We then examined whether overexpression of TrkB in corticospinal neurons affected axon collateral
612 arborization in the pons. pCAGGS-TrkB-V5 was transfected alone or together with pCAGGS-PTPRO-FLAG
613 or pCAGGS-PTPRO^{DA}-FLAG by IUE at E12.5 (Fig. 6*C*). Fluorescence intensity analysis revealed that TrkB
614 overexpression significantly increased collateral arborization compared with Mock controls, whereas co-
615 expression of wild-type PTPRO substantially reduced this increase, and PTPRO^{DA} failed to suppress TrkB-
616 induced arborization [one-way ANOVA followed by Tukey's multiple-comparisons test; Mock vs TrkB, TrkB

JNeurosci Accepted Manuscript

vs TrkB+PTPRO, TrkB+PTPRO vs TrkB+PTPRO^{DA}; bin 1, $F(3, 20) = 10.63$, ANOVA $p = 0.0002$, Tukey-adjusted $p = 0.0274$, $p = 0.0013$, $p = 0.0008$; bin 2, $F(3, 20) = 9.594$, ANOVA $p = 0.0004$, Tukey-adjusted $p = 0.0298$, $p = 0.0009$, $p = 0.0024$] (Fig. 6*D*). To further characterize collateral morphology at the single-axon level, sparse labeling was performed (Fig. 6*E*). The number of collaterals per axon was not significantly different between TrkB-overexpressing and Mock groups (Fig. S6*D*). However, the number of branches per collateral was significantly increased in TrkB-overexpressing neurons compared with Mock controls [Welch's *t* test, $t(6.036) = 9.736$, $p < 0.0001$] (Fig. S6*E*). TrkB overexpression significantly increased the numbers of primary, secondary, and tertiary branches, whereas quaternary and quinary branches showed no significant difference [primary, Welch's *t* test, $t(5.571) = 6.356$, $p = 0.0009$; secondary, Welch's *t* test, $t(7.451) = 6.709$, $p = 0.0002$; tertiary, two-tailed Mann–Whitney U test, $U = 2.500$, $p = 0.0476$] (Fig. 6*F*). Collateral complexity index was also significantly higher in TrkB-overexpressing collaterals than in Mock controls [Welch's *t* test, $t(5.223) = 9.867$, $p = 0.0001$] (Fig. 6*G*). When collateral branch distribution was analyzed along the dorsoventral axis, branch numbers in bins 1, 2, 3, and 4 were significantly increased in TrkB-overexpressing collaterals compared with Mock controls [bin 1, Welch's *t* test, $t(6.682) = 7.364$, $p = 0.0002$; bin 2, Welch's *t* test, $t(7.131) = 6.537$, $p = 0.0003$; bin 3, Welch's *t* test, $t(4.731) = 6.661$, $p = 0.0014$; bin 4, two-tailed Mann–Whitney U test, $U = 1.500$, $p = 0.0317$] (Fig. 6*H*). To further confirm that the arborization effect of *Ptpro* knockdown was mediated through TrkB signaling, we performed double knockdown experiments using sh*Ptpro* and sh*Ntrk2* (which encodes TrkB) (Figs. 6*I* and S6*C*). The increase in collateral fluorescence intensity observed in sh*Ptpro*-transfected axons was significantly attenuated by co-transfection with sh*Ntrk2* [one-way ANOVA followed by Tukey's multiple-comparisons test; sh*Ptpro* vs sh*Ptpro*+sh*Ntrk2*; bin 1, $F(3, 20) = 40.51$, ANOVA $p < 0.0001$, Tukey-adjusted $p < 0.0001$; bin 2, $F(3, 20) = 38.83$, ANOVA $p < 0.0001$, Tukey-adjusted $p < 0.0001$; bin 3, $F(3, 20) = 42.14$, ANOVA $p < 0.0001$, Tukey-adjusted $p < 0.0001$; bin 4, $F(3, 20) = 32.27$, ANOVA $p < 0.0001$, Tukey-adjusted $p < 0.0001$; bin 5, $F(3, 20) = 22.49$, ANOVA $p < 0.0001$, Tukey-adjusted $p < 0.0001$; bin 6, $F(3, 20) = 14.77$, ANOVA $p < 0.0001$, Tukey-adjusted $p = 0.0001$] (Fig. 6*I*, *J*). Taken together, these results indicate that PTPRO suppresses axon collateral arborization in the pons through inhibition of TrkB signaling. The increase in collateral fluorescence caused by *Ptpro* knockdown was attenuated by simultaneous *Ntrk2* knockdown, supporting a role for TrkB signaling in the regulatory effect of PTPRO.

JNeurosci Accepted Manuscript

PTPRO restricted axon collateral arborization through inhibition of TrkB-PI3K signaling

TrkB activation triggers PI3K signaling, which plays a critical role in promoting axon collateral branching through localized cytoskeletal reorganization (Gallo and Letourneau, 1998; Ketschek and Gallo, 2010; Cheng et al., 2011). TrkB-mediated axonal growth has been shown to involve both PI3K and MEK signaling pathways downstream of the Shc binding site of TrkB (Atwal et al., 2000). To determine whether PTPRO regulates collateral arborization through PI3K signaling downstream of TrkB, we administered the PI3K inhibitor BKM120 by intragastric injection at P0, P1, and P2 to pups that had undergone IUE at E12.5 with sh*Ptpro* or sh*Scramble* together with a tdTomato expression plasmid (Pitulescu et al., 2010) (Fig. 7*A*). BKM120 was selected over LY294002, a commonly used PI3K inhibitor, due to its longer half-life and blood-brain barrier permeability (Maira et al., 2012; Speranza et al., 2016). Fluorescence intensity analysis revealed that sh*Ptpro*+Vehicle collaterals showed significantly higher arborization in bins 1-3, 5, and 6 compared with sh*Scramble*+Vehicle controls, and this increase was significantly attenuated by BKM120 administration in the sh*Ptpro*+BKM120 group [one-way ANOVA followed by Tukey's multiple-comparisons test; sh*Ptpro* vs sh*Ptpro*+BKM120; bin 1, $F(3, 20) = 17.24$, ANOVA $p < 0.0001$, Tukey-adjusted $p = 0.0001$; bin 2, $F(3, 20) = 18.63$, ANOVA $p < 0.0001$, Tukey-adjusted $p = 0.0002$; bin 3, $F(3, 20) = 10.08$, ANOVA $p = 0.0003$, Tukey-adjusted $p = 0.0050$; bin 5, $F(3, 20) = 7.139$, ANOVA $p = 0.0019$, Tukey-adjusted $p = 0.0097$; bin 6, $F(3, 20) = 4.904$, ANOVA $p = 0.0103$, Tukey-adjusted $p = 0.0197$] (Fig. 7*B*, *C*). At the single-axon level (Fig. 7*D*), the number of collaterals per axon was not significantly different among all four groups (Fig. S6*F*). However, the number of branches per collateral and collateral complexity index were significantly increased in sh*Ptpro*+Vehicle collaterals compared with controls, and these increases were reduced by BKM120 treatment [Welch's one-way ANOVA followed by Tamhane's T2 multiple-comparisons test; sh*Ptpro* + Vehicle vs sh*Ptpro* + BKM120; branches per collateral, $W(3, 10.59) = 7.023$, Welch ANOVA $p = 0.0071$, Tamhane-adjusted $p = 0.0383$; collateral complexity index, $W(3, 10.53) = 6.674$, Welch ANOVA $p = 0.0086$, Tamhane-adjusted $p = 0.0422$] (Fig. 7*E*, *F*). Branch numbers for primary, secondary, tertiary and quaternary were all significantly increased in sh*Ptpro*+Vehicle collaterals, and BKM120 treatment significantly reduced these increases [sh*Ptpro* + Vehicle vs sh*Ptpro* + BKM120; Welch's one-way ANOVA followed by Tamhane's T2 multiple-comparisons test; primary, $W(3, 10.46) = 11.21$, Welch ANOVA $p = 0.0013$, Tamhane-adjusted $p = 0.0226$; Kruskal–Wallis test followed by Dunn's multiple-comparisons test;

JNeurosci Accepted Manuscript

secondary, $H(3) = 13.38$, Kruskal–Wallis $p = 0.0039$, Dunn-adjusted $p = 0.0472$; tertiary, $H(3) = 20.38$, Kruskal–Wallis $p = 0.0001$, Dunn-adjusted $p = 0.0048$; quaternary, $H(3) = 17.84$, Kruskal–Wallis $p = 0.0005$, Dunn-adjusted $p = 0.0034$] (Fig. 7*G*). When analyzed along the dorsoventral axis, collateral branch numbers in bins 1-3 were significantly higher in sh*Ptpro*+Vehicle collaterals, and BKM120 treatment significantly attenuated this arborization [sh*Ptpro* + Vehicle vs sh*Ptpro* + BKM120; one-way ANOVA followed by Tukey's multiple-comparisons test; bin 1, $F(3, 20) = 27.78$, ANOVA $p < 0.0001$, Tukey-adjusted $p < 0.0001$; Kruskal–Wallis test followed by Dunn's multiple-comparisons test; bin 2, $H(3) = 12.41$, Kruskal–Wallis $p = 0.0061$, Dunn-adjusted $p = 0.0277$; bin 3, $H(3) = 14.06$, Kruskal–Wallis $p = 0.0028$, Dunn-adjusted $p = 0.0378$] (Fig. 7*H*). Taken together, these results demonstrate that PTPRO suppresses axon collateral arborization through inhibition of TrkB-PI3K signaling, and that the enhanced collateral arborization induced by *Ptpro* knockdown is mediated through activation of the PI3K pathway downstream of TrkB.

JNeurosci Accepted Manuscript

Discussion

In this study, we demonstrate that PTPRO negatively regulates the complexity of axon collateral arborization of corticopontine projections, rather than collateral initiation. Knockdown of *Ptpro* in L5 corticospinal neurons increased both the number of branches per collateral and the complexity of collateral arbors in the pons (Figs. 2 and 3), while overexpression of PTPRO suppressed collateral arborization (Fig. 5). This regulatory function depends on the intracellular phosphatase activity of PTPRO (Fig. 4*B*–*D*) and operates through inhibition of TrkB-PI3K signaling (Figs. 6 and 7). These findings identify PTPRO as a cell-intrinsic brake on corticopontine terminal arbor elaboration.

Previous work reported *Ptpro* expression in the upper layers of the frontal cortex at P2 (Beltran et al., 2003), while single-cell transcriptomic data indicated its presence in L5 at E14.5 and P0 (Loo et al., 2019). However, a systematic characterization of *Ptpro* across cortical layers and developmental stages was lacking. By combining ISH with IHC, we confirmed that *Ptpro* is robustly co-expressed with the L5 marker Ctip2 in frontal and parietal cortex at P0, with weaker expression in the occipital cortex (Figs. 1*A*–*C* and S1*D*). RT-PCR further showed that the long-form splice variant was continuously expressed in *Fezf2*-positive L5 neurons from E13 through P0 (Fig. S1*E*), during the period when corticopontine collaterals arise and elaborate (Inoue et al., 1992; Leergaard and Bjaalie, 2007). This temporal and spatial expression pattern places PTPRO in an ideal position to regulate collateral arborization.

A key finding of this study is that PTPRO selectively controls higher-order branching complexity rather than collateral initiation. Sparse labeling analysis revealed that *Ptpro* knockdown increased branch numbers per collateral and elevated collateral complexity index without affecting the number of collaterals per axon (Figs. 3*E*, *F*, and S4*B*, *F*, *H*, *I*). Overexpression of PTPRO produced the mirror phenotype: reduced branches per collateral and collateral complexity index with no change in collateral number (Fig. 5D–*G*). This selectivity is important because collateral initiation and terminal arbor elaboration are likely governed by distinct molecular programs. Previous work in trigeminal ganglion neurons showed that PTPRO restricts overall axon elongation and branching by repressing TrkB and Ret signaling (Gatto et al., 2013). Our results reveal a more refined role for PTPRO in the CNS: rather than broadly suppressing axon growth, PTPRO specifically tunes the higher-order branching that determines terminal arbor architecture.

JNeurosci Accepted Manuscript

One possible explanation for this selectivity is that collateral initiation and higher-order branching rely on distinct intracellular signaling thresholds and spatial dynamics. Initial collateral formation may be triggered by local cytoskeletal destabilization and guidance cue signaling, whereas higher-order branching requires sustained activation of growth-promoting pathways such as TrkB-PI3K signaling. Because PTPRO attenuates TrkB phosphorylation at the receptor level, its effect would be expected to preferentially influence signaling-dependent amplification of branches rather than the initial emergence of collateral protrusions.

It is also noteworthy that the effect of *Ptpro* knockdown was prominent in motor and somatosensory corticopontine projections but absent in auditory cortex projections (Figs. 2*D*–*G*, S2*G*, *H* and S3*A*-*F*), suggesting that PTPRO-mediated regulation of collateral complexity is area specific. This regional difference may reflect variations in *Ptpro* expression levels or differences in the responsiveness of corticopontine axons to neurotrophin signaling. Among these possibilities, differential activation of TrkB signaling may be particularly important. Even within a common target such as the pons, corticopontine axons originating from different cortical areas may exhibit distinct sensitivities to BDNF–TrkB signaling. In regions such as the motor and somatosensory cortex, where TrkB signaling may be more effectively engaged, PTPRO-mediated dephosphorylation of TrkB would have a stronger impact on suppressing collateral arborization. In contrast, reduced TrkB responsiveness in auditory projections may render PTPRO functionally less influential. This raises the possibility that cortical area identity is translated into distinct terminal arbor architectures through differential tuning of TrkB signaling sensitivity. However, TrkB activation was not directly compared across cortical areas, and this interpretation therefore remains hypothetical. Whether this mechanism extends beyond the corticopontine system remains unknown. Other long-range projection pathways, including corticothalamic, corticostriatal, and corticocortical projections, also exhibit area-specific differences in terminal arbor architecture, raising the possibility that related regulatory mechanisms may operate in these systems. Future studies examining PTPRO function in other projection pathways will be required to determine the generality of the mechanism identified here.

Structure-function analysis showed that the phosphatase activity of PTPRO is essential for its role in collateral arborization, whereas the extracellular fibronectin type III-like domains are dispensable. Co-expression of an shRNA-resistant PTPRO lacking the extracellular domain rescued the *Ptpro* knockdown phenotype, but the phosphatase-dead mutant PTPRO^{DA} did not (Fig. 4*B*–*D*). This contrasts with the

JNeurosci Accepted Manuscript

requirement of the extracellular domains for PTPRO-mediated synapse formation (Jiang et al., 2017), indicating that PTPRO engages distinct functional domains to regulate different aspects of neural circuit assembly. The intracellular phosphatase domain has previously been implicated in regulating retinal axon sensitivity to ephrins (Shintani et al., 2006) and in nerve growth factor (NGF)-induced neurite outgrowth through dephosphorylation of neuronal pentraxin with chromo domain (NPCD) (Chen and Bixby, 2005a, 2005b). Our results add terminal arbor regulation to the repertoire of phosphatase-dependent functions of PTPRO.

An intriguing aspect of PTPRO regulation concerns its dimerization state. Monomeric PTPRO is enzymatically active, whereas dimerization inhibits phosphatase activity (Hower et al., 2009). The juxtamembrane domain, which differs between the long-form and short-form splice variants by 28 amino acids, may contribute to this dimerization. We found that the long-form variant predominates in L5 neurons during early development (E13–P0), while the short form begins to appear at P0 (Fig. S1*E*). Because corticopontine collaterals arise and elaborate during the perinatal period (Inoue et al., 1992; Leergaard and Bjaalie, 2007), it is tempting to speculate that a developmental shift from long-form to short-form expression alters the dimerization equilibrium of PTPRO, thereby modulating its phosphatase activity and fine-tuning collateral arborization. Future studies examining how splice variant switching affects PTPRO dimerization and downstream signaling will be important for understanding this regulatory mechanism.

Our findings support TrkB as a downstream target of PTPRO in the regulation of collateral arborization. Co-immunoprecipitation showed that PTPRO interacted with TrkB, and wild-type PTPRO markedly reduced TrkB phosphotyrosine levels, whereas PTPRO^{DA} did not (Fig. 6*A*, *B*). Functionally, the enhanced arborization induced by TrkB overexpression was suppressed by wild-type PTPRO but not by PTPRO^{DA} (Fig. 6*C*, *D*), and the excessive branching caused by *Ptpro* knockdown was attenuated by simultaneous depletion of TrkB (Fig. 6*I*, *J*). Pharmacological inhibition of PI3K with BKM120 similarly reversed the *Ptpro* knockdown phenotype at both the population and single-axon levels (Fig. 7*B*–*H*) without affecting collateral number (Fig. S6*F*), supporting a PTPRO-TrkB-PI3K signaling axis. Within the broader framework of growth-promoting and growth-restricting signals that shape collateral arborization, PTPRO occupies a distinct position. PTEN constrains neuronal arborization by antagonizing PI3K at the level of lipid products (Kwon et al., 2006), whereas PTPRO operates upstream by dephosphorylating TrkB, thereby attenuating signaling

JNeurosci Accepted Manuscript

at the receptor level. This receptor-proximal mode of action positions PTPRO as a checkpoint that sets the upper boundary of TrkB-PI3K-driven branch complexity before the signal propagates to downstream effectors. Although our data identify TrkB as a major downstream target of PTPRO in this context, it remains possible that additional receptor tyrosine kinases or signaling pathways also contribute to the regulation of collateral arborization.

Corticopontine collateral arborization establishes the synaptic connections between individual corticospinal neurons and their target pontine neurons (Gallo, 2011; Iguchi et al., 2021). The branching pattern of these collaterals is therefore likely to determine the precision of corticopontine connectivity. Our finding that PTPRO constrains terminal arbor complexity suggests that it contributes to the formation of appropriately sized synaptic territories for each cortical input. Differences in terminal arbor complexity may directly influence the strength and convergence of cortical inputs onto pontine neurons, thereby shaping the fidelity and gain of cerebro-cerebellar information transfer. Future investigations should address which specific branches form functional synapses with pontine neurons, how the branching pattern shaped by PTPRO affects information relay at the pontine level, and whether similar phosphatase-dependent mechanisms operate in other projection systems where terminal arbor complexity varies across target regions. Together, these results establish PTPRO-TrkB-PI3K signaling as a key molecular pathway that selectively governs higher-order branching during corticopontine terminal arbor elaboration, providing a mechanistic framework for how projection-specific arbor complexity is achieved in the central nervous system.

JNeurosci Accepted Manuscript

References

Aiyar A, Xiang Y, Leis J (1996) Site-directed mutagenesis using overlap extension PCR. Methods Mol Biol 57:177–191.

Arlotta P, Molyneaux BJ, Chen J, Inoue J, Kominami R, Macklis JD (2005) Neuronal subtype-specific genes that control corticospinal motor neuron development in vivo. Neuron 45:207–221.

Atwal JK, Massie B, Miller FD, Kaplan DR (2000) The TrkB-Shc site signals neuronal survival and local axon growth via MEK and PI3-kinase. Neuron 27:265–277.

Bastmeyer M, O'Leary DD (1996) Dynamics of target recognition by interstitial axon branching along developing cortical axons. J Neurosci Off J Soc Neurosci 16:1450–1459.

Beltran PJ, Bixby JL, Masters BA (2003) Expression of PTPRO during mouse development suggests involvement in axonogenesis and differentiation of NT-3 and NGF-dependent neurons. J Comp Neurol 456:384–395.

Chen B, Bixby JL (2005a) A Novel Substrate of Receptor Tyrosine Phosphatase PTPRO Is Required for Nerve Growth Factor-Induced Process Outgrowth. J Neurosci 25:880–888.

Chen B, Bixby JL (2005b) Neuronal pentraxin with chromo domain (NPCD) is a novel class of protein expressed in multiple neuronal domains. J Comp Neurol 481:391–402.

Cheng P-L, Song A-H, Wong Y-H, Wang S, Zhang X, Poo M-M (2011) Self-amplifying autocrine actions of BDNF in axon development. Proc Natl Acad Sci U S A 108:18430–18435.

Clare AJ, Day RC, Empson RM, Hughes SM (2018) Transcriptome Profiling of Layer 5 Intratelencephalic Projection Neurons From the Mature Mouse Motor Cortex. Front Mol Neurosci 11:410.

Cohen-Cory S, Kidane AH, Shirkey NJ, Marshak S (2010) Brain-derived neurotrophic factor and the development of structural neuronal connectivity. Dev Neurobiol 70:271–288.

Dascenco D, Erfurth M-L, Izadifar A, Song M, Sachse S, Bortnick R, Urwyler O, Petrovic M, Ayaz D, He H, Kise Y, Thomas F, Kidd T, Schmucker D (2015) Slit and Receptor Tyrosine Phosphatase 69D Confer Spatial Specificity to Axon Branching via Dscam1. Cell 162:1140–1154.

Eckler MJ, Larkin KA, McKenna WL, Katzman S, Guo C, Roque R, Visel A, Rubenstein JLL, Chen B (2014) Multiple conserved regulatory domains promote Fezf2 expression in the developing cerebral cortex. Neural Develop 9:6.

JNeurosci Accepted Manuscript

819 Flint AJ, Tiganis T, Barford D, Tonks NK (1997) Development of “substrate-trapping” mutants to identify
820 physiological substrates of protein tyrosine phosphatases. Proc Natl Acad Sci U S A 94:1680–1685.
821 Gallo G (2011) The cytoskeletal and signaling mechanisms of axon collateral branching. Dev Neurobiol
822 71:201–220.
823 Gallo G, Letourneau PC (1998) Localized sources of neurotrophins initiate axon collateral sprouting. J
824 Neurosci Off J Soc Neurosci 18:5403–5414.
825 Gatto G, Dudanova I, Suetterlin P, Davies AM, Drescher U, Bixby JL, Klein R (2013) Protein tyrosine
826 phosphatase receptor type O inhibits trigeminal axon growth and branching by repressing TrkB and
827 Ret signaling. J Neurosci Off J Soc Neurosci 33:5399–5410.
828 Gong S, Zheng C, Doughty ML, Losos K, Didkovsky N, Schambra UB, Nowak NJ, Joyner A, Leblanc G,
829 Hatten ME, Heintz N (2003) A gene expression atlas of the central nervous system based on
830 bacterial artificial chromosomes. Nature 425:917–925.
831 Hower AE, Beltran PJ, Bixby JL (2009) Dimerization of tyrosine phosphatase PTPRO decreases its
832 activity and ability to inactivate TrkC. J Neurochem 110:1635–1647.
833 Hsu S, Motiwala T, Roy S, Claus R, Mustafa M, Plass C, Freitas MA, Ghoshal K, Jacob ST (2013)
834 Methylation of the PTPRO gene in human hepatocellular carcinoma and identification of VCP as its
835 substrate. J Cell Biochem 114:1810–1818.
836 Iguchi T, Oka Y, Yasumura M, Omi M, Kuroda K, Yagi H, Xie M-J, Taniguchi M, Bastmeyer M, Sato M
837 (2021) Mutually Repulsive EphA7-EfnA5 Organize Region-to-Region Corticopontine Projection by
838 Inhibiting Collateral Extension. J Neurosci Off J Soc Neurosci 41:4795–4808.
839 Inoue K, Terashima T, Inoue Y (1992) Postnatal Development of the Corticotectal Projection from the
840 Visual Cortex of the Mouse. Okajimas Folia Anat Jpn 68:319–331.
841 Jaworski J, Spangler S, Seeburg DP, Hoogenraad CC, Sheng M (2005) Control of Dendritic Arborization
842 by the Phosphoinositide-3′-Kinase–Akt–Mammalian Target of Rapamycin Pathway. J Neurosci
843 25:11300–11312.
844 Jiang W, Wei M, Liu M, Pan Y, Cao D, Yang X, Zhang C (2017) Identification of Protein Tyrosine
845 Phosphatase Receptor Type O (PTPRO) as a Synaptic Adhesion Molecule that Promotes Synapse
846 Formation. J Neurosci Off J Soc Neurosci 37:9828–9843.

JNeurosci Accepted Manuscript

847 Johnson KG, Van Vactor D (2003) Receptor protein tyrosine phosphatases in nervous system
848 development. Physiol Rev 83:1–24.
849 Kalil K, Dent EW (2014) Branch management: mechanisms of axon branching in the developing
850 vertebrate CNS. Nat Rev Neurosci 15:7–18.
851 Ke M-T, Nakai Y, Fujimoto S, Takayama R, Yoshida S, Kitajima TS, Sato M, Imai T (2016) Super-
852 Resolution Mapping of Neuronal Circuitry With an Index-Optimized Clearing Agent. Cell Rep
853 14:2718–2732.
854 Ketschek A, Gallo G (2010) Nerve growth factor induces axonal filopodia through localized microdomains
855 of phosphoinositide 3-kinase activity that drive the formation of cytoskeletal precursors to filopodia. J
856 Neurosci Off J Soc Neurosci 30:12185–12197.
857 Krueger NX, Saito H (1992) A human transmembrane protein-tyrosine-phosphatase, PTP zeta, is
858 expressed in brain and has an N-terminal receptor domain homologous to carbonic anhydrases. Proc
859 Natl Acad Sci U S A 89:7417–7421.
860 Kwon C-H, Luikart BW, Powell CM, Zhou J, Matheny SA, Zhang W, Li Y, Baker SJ, Parada LF (2006)
861 Pten regulates neuronal arborization and social interaction in mice. Neuron 50:377–388.
862 Leergaard TB, Bjaalie JG (2007) Topography of the complete corticopontine projection: from experiments
863 to principal Maps. Front Neurosci 1:211–223.
864 Loo L, Simon JM, Xing L, McCoy ES, Niehaus JK, Guo J, Anton ES, Zylka MJ (2019) Single-cell
865 transcriptomic analysis of mouse neocortical development. Nat Commun 10:134.
866 Maira S-M et al. (2012) Identification and characterization of NVP-BKM120, an orally available pan-class I
867 PI3-kinase inhibitor. Mol Cancer Ther 11:317–328.
868 Marshak S, Nikolakopoulou AM, Dirks R, Martens GJ, Cohen-Cory S (2007) Cell-autonomous TrkB
869 signaling in presynaptic retinal ganglion cells mediates axon arbor growth and synapse maturation
870 during the establishment of retinotectal synaptic connectivity. J Neurosci Off J Soc Neurosci
871 27:2444–2456.
872 Mihailoff GA, Adams CE, Woodward DJ (1984) An autoradiographic study of the postnatal development
873 of sensorimotor and visual components of the corticopontine system. J Comp Neurol 222:116–127.

JNeurosci Accepted Manuscript

874 Molyneaux BJ, Arlotta P, Hirata T, Hibi M, Macklis JD (2005) Fezl Is Required for the Birth and
875 Specification of Corticospinal Motor Neurons. Neuron 47:817–831.
876 Motiwala T, Datta J, Kutay H, Roy S, Jacob ST (2010) Lyn kinase and ZAP70 are substrates of PTPROt
877 in B-cells: Lyn inactivation by PTPROt sensitizes leukemia cells to VEGF-R inhibitor pazopanib. J
878 Cell Biochem 110:846–856.
879 Muzumdar MD, Tasic B, Miyamichi K, Li L, Luo L (2007) A global double-fluorescent Cre reporter mouse.
880 Genesis 45:593–605.
881 Nagano T, Yoneda T, Hatanaka Y, Kubota C, Murakami F, Sato M (2002) Filamin A-interacting protein
882 (FILIP) regulates cortical cell migration out of the ventricular zone. Nat Cell Biol 4:495–501.
883 Nguyen MQ, Taniguchi M, Yasumura M, Iguchi T, Sato M (2022) Cytoneme-like protrusion formation
884 induced by LAR is promoted by receptor dimerization. Biol Open 11:bio059024.
885 Niwa H, Yamamura K, Miyazaki J (1991) Efficient selection for high-expression transfectants with a novel
886 eukaryotic vector. Gene 108:193–199.
887 Oka Y, Doi M, Taniguchi M, Tiong SYX, Akiyama H, Yamamoto T, Iguchi T, Sato M (2021) Interstitial
888 Axon Collaterals of Callosal Neurons Form Association Projections from the Primary Somatosensory
889 to Motor Cortex in Mice. Cereb Cortex 31:5225–5238.
890 O'Leary DD, Terashima T (1988) Cortical axons branch to multiple subcortical targets by interstitial axon
891 budding: implications for target recognition and "waiting periods." Neuron 1:901–910.
892 Pitulescu ME, Schmidt I, Benedito R, Adams RH (2010) Inducible gene targeting in the neonatal
893 vasculature and analysis of retinal angiogenesis in mice. Nat Protoc 5:1518–1534.
894 Potts EM, Coppotelli G, Ross JM (2020) Histological-Based Stainings using Free-Floating Tissue
895 Sections. J Vis Exp JoVE.
896 Sahni V, Shnider SJ, Jabaudon D, Song JHT, Itoh Y, Greig LC, Macklis JD (2021) Corticospinal neuron
897 subpopulation-specific developmental genes prospectively indicate mature segmentally specific axon
898 projection targeting. Cell Rep 37:109843.
899 Sato M, Lopez-Mascaraque L, Heffner CD, O'Leary DD (1994) Action of a diffusible target-derived
900 chemoattractant on cortical axon branch induction and directed growth. Neuron 13:791–803.

JNeurosci Accepted Manuscript

Shaner NC, Campbell RE, Steinbach PA, Giepmans BNG, Palmer AE, Tsien RY (2004) Improved monomeric red, orange and yellow fluorescent proteins derived from Discosoma sp. red fluorescent protein. Nat Biotechnol 22:1567–1572.

Shintani T, Ihara M, Sakuta H, Takahashi H, Watakabe I, Noda M (2006) Eph receptors are negatively controlled by protein tyrosine phosphatase receptor type O. Nat Neurosci 9:761–769.

Speranza M-C, Nowicki MO, Behera P, Cho C-F, Chiocca EA, Lawler SE (2016) BKM-120 (Buparlisib): A Phosphatidyl-Inositol-3 Kinase Inhibitor with Anti-Invasive Properties in Glioblastoma. Sci Rep 6:20189.

Stepanek L, Sun QL, Wang J, Wang C, Bixby JL (2001) CRYP-2/cPTPRO is a neurite inhibitory repulsive guidance cue for retinal neurons in vitro. J Cell Biol 154:867–878.

Stoker AW (2001) Receptor tyrosine phosphatases in axon growth and guidance. Curr Opin Neurobiol 11:95–102.

Suzuki SC, Inoue T, Kimura Y, Tanaka T, Takeichi M (1997) Neuronal circuits are subdivided by differential expression of type-II classic cadherins in postnatal mouse brains. Mol Cell Neurosci 9:433–447.

Tagawa M, Shirasawa T, Yahagi Y, Tomoda T, Kuroyanagi H, Fujimura S, Sakiyama S, Maruyama N (1997) Identification of a receptor-type protein tyrosine phosphatase expressed in postmitotic maturing neurons: its structure and expression in the central nervous system. Biochem J 321 (Pt 3):865–871.

Taniguchi M, Iwahashi M, Oka Y, Tiong SYX, Sato M (2022) Fezf2-positive fork cell-like neurons in the mouse insular cortex. PloS One 17:e0274170.

Tautz L, Critton DA, Grotegut S (2013) Protein tyrosine phosphatases: structure, function, and implication in human disease. Methods Mol Biol 1053:179–221.

Winnubst J et al. (2019) Reconstruction of 1,000 Projection Neurons Reveals New Cell Types and Organization of Long-Range Connectivity in the Mouse Brain. Cell 179:268-281.e13.

Yagi H, Oka Y, Komada M, Xie M-J, Noguchi K, Sato M (2016) Filamin A interacting protein plays a role in proper positioning of callosal projection neurons in the cortex. Neurosci Lett 612:18–24.

JNeurosci Accepted Manuscript

928 Zhu Y, Matsumoto T, Mikami S, Nagasawa T, Murakami F (2009) SDF1/CXCR4 signalling regulates two
929 distinct processes of precerebellar neuronal migration and its depletion leads to abnormal pontine
930 nuclei formation. Development 136:1919–1928.
931
932

JNeurosci Accepted Manuscript

933 **Figure legends**

934

935 **Figure 1. *Ptpro* was expressed in L5 cortical neurons in developing mouse brain.**

936 ***A***, *Ptpro* expression was detected by *in situ* hybridization (ISH) in the somatosensory, motor, visual, and
937 auditory cortices at postnatal day 0 (P0), with comparatively lower expression in the visual and auditory
938 cortices. M, motor cortex. S, somatosensory cortex. V, visual cortex. A, auditory cortex. Scale bar, 500 μm.
939 ***B***, ***C***, *Ptpro* was concentrated in layer (L) 2/3, L4, and L5 cortical neurons in the frontal and parietal regions
940 but was only faintly expressed in L5 neurons in the occipital region. *Ptpro* ISH (purple), Ctip2
941 immunohistochemistry (IHC; brown), and the merged images in parietal (***B***) and occipital (***C***) cortex. Red
942 boxed areas are shown at higher magnification in the adjacent panels. Red arrowheads identify L5 neurons
943 positive for both *Ptpro* and Ctip2. R, rostral; C, caudal. WM, white matter. Scale bars, 500 μm, 200 μm, 100
944 μm in left, middle, right panel, respectively.

945

946 **Figure 2. Knockdown of *Ptpro* resulted in increased corticospinal collateral signal in the pons.**

947 ***A***, Image of the brain transfected with plasmids. shRNA and tdTomato expression vectors were co-
948 transfected into L5 cortical neurons by *in utero* electroporation (IUE) at embryonic day (E) 12.5. Scale bar,
949 2 mm. ***B***, Experimental timeline for IUE at E12.5 and analysis of parasagittal brain sections at P1 or P2. ***C,***
950 Schematic of the fluorescence intensity analysis. The pontine region between the lower edge of the
951 corticospinal axon main shaft and the ventral boundary of the pons was divided into 10 equal dorsoventral
952 bins. ***D***, ***F***, Representative P2 corticopontine projections from motor (***D***) and somatosensory (***F***) cortex after
953 transfection with sh*Scramble* or sh*Ptpro*. The white dashed line delineates the ventral boundary of the pons,
954 and the labeled oblique tract is the axon main shaft used for normalization. Scale bars, 200 μm. ***E***, ***G***,
955 Quantification of the images in (***D***) and (***F***), respectively. Fluorescence intensity in each bin was normalized
956 to that of the axon main shaft. Values are normalized to axon main shaft and shown as the mean ± SEM.
957 Welch's *t* test, **p* < 0.05, ***p* < 0.01, ****p* < 0.001. ***E***, *n* = 4 mice per group; ***G***, *n* = 6 mice per group. ***H***,
958 Representative somatosensory projections after transfection with sh*Scramble*, sh*Ptpro* + empty vector

Neurosci Accepted Manuscript

(Mock), or sh*Ptpro* + shRNA-resistant *Ptpro* (*Ptpro*-res). Scale bar, 200 μm. ***I***, Quantification of the images in (***H***). *n* = 6 mice per group. Values are normalized to axon main shaft and shown as the mean ± SEM. One-way ANOVA followed by Tukey's multiple-comparisons test, **p* < 0.05, ***p* < 0.01, ****p* < 0.001. The mouse was used as the statistical unit.

Figure 3. Acute deficiency of *Ptpro* resulted in the enhancement of axon collateral arborization in the pons.

A, Schematic drawing of the pCAG-DIO-iCre for sparse labeling. Triangles, P, loxP; 2, lox2272. WPRE, woodchuck hepatitis virus post-transcriptional regulatory element. polyA, rabbit β-globin 3'UTR sequence. ***B***, Tissues were optically cleared with SeeDB2 to facilitate imaging the labeled axon collaterals. Scale bars, 2 mm. ***C***, Representative traced EGFP-positive corticopontine axons and collateral arbors from sh*Scramble* and sh*Ptpro* groups. Red boxes delimit the collateral regions enlarged in the middle panels. The right panels show individual collateral arbors, and red arrowheads mark branch points. The white dashed line delineates the pons. Scale bars, 50 μm. ***D***, Schematic of branch-order classification. A collateral emerging from the main axonal shaft was designated as order 0. Branches arising from its first bifurcation were defined as primary branches, and each subsequent bifurcation increased the branch order by one. ***E***, Quantification of branch numbers at each branch order. ***F***, Formula for the collateral complexity index, adapted from a previous study (Marshak et al., 2007), and quantification of the collateral complexity index for each mouse. ***G***, The region of the pons underneath the corticospinal axonal shaft was evenly divided into 5 bins along the vertical axis. ***H***, Quantification of branch numbers in each dorsoventral bin. ***E***, ***F***, ***H***, *n* = 8 mice per group. Values represent the mean ± SEM. Welch's *t* test or Mann–Whitney *U* test, depending on data normality and homogeneity of variance. **p* < 0.05, ***p* < 0.01, ****p* < 0.001. The mouse was used as the statistical unit.

Figure 4. PTPRO phosphatase activity was required to suppress axon collateral arborization in the pons.

JNeurosci Accepted Manuscript

A, Schematic structures of PTPRO and its mutants. Domain organization of wild-type PTPRO, the phosphatase-dead substrate-trapping mutant $PTPRO^{DA}$ (D1112A), and the N-terminal deletion mutant $PTPRO^{NTD}$. FNIII, fibronectin type III domain; TM, transmembrane domain. ***B***, Representative P2 somatosensory corticopontine projections after *Ptpro* knockdown combined with Mock, shRNA-resistant wild-type PTPRO (*Ptpro*-res), $PTPRO^{DA}$, or $PTPRO^{NTD}$. The white dashed line delineates the pons, and the labeled tract is the axon main shaft. Scale bar, 200 μm. ***C***, Quantification of the images in (***B***) comparing rescue by *Ptpro*-res with the phosphatase-dead mutant. ***D***, Quantification of the images in (***B***) comparing rescue by *Ptpro*-res with the extracellular-domain deletion mutant. ***C***, ***D***, n = 6 mice per group. Values are normalized to axon main shaft and shown as the mean ± SEM. One-way ANOVA followed by Tukey's multiple-comparisons test. *$p < 0.05$, **$p < 0.01$. The mouse was used as the statistical unit.

Figure 5. Overexpression of PTPRO resulted in decreased axon collateral arborization in the pons.

A, Representative P2 somatosensory corticopontine projections after overexpression of Mock, wild-type PTPRO, $PTPRO^{DA}$, or $PTPRO^{NTD}$. The white dashed line delineates the pons, and the labeled tract is the axon main shaft. Scale bar, 200 μm. ***B***, Quantification of the images in (***A***). Fluorescence intensity in each of 10 dorsoventral bins was normalized to that of the axon main shaft. ***C***, Representative traced EGFP-positive corticopontine axons and collateral arbors from Mock, PTPRO, $PTPRO^{DA}$, or $PTPRO^{NTD}$ groups. Red arrowheads mark collateral branch points, and the white dashed line delineates the pons. Scale bar, 100 μm. ***D***, Quantification of the mean number of collaterals per axon. ***E***, Quantification of the mean number of branches per collateral. ***F***, Quantification of the collateral complexity index for each mouse. ***G***, Quantification of branch numbers at each branch order. ***H***, Quantification of branch numbers in each dorsoventral bin. ***B***, ***D***-***H***, n = 6 mice per group. Values represent the mean ± SEM. One-way ANOVA followed by Tukey's multiple-comparisons test or Kruskal–Wallis test followed by Dunn's multiple-comparisons test, depending on data normality and homogeneity of variance. *$p < 0.05$, **$p < 0.01$, ***$p < 0.001$. ns, not significant. The mouse was used as the statistical unit.

JNeurosci Accepted Manuscript

Figure 6. PTPRO suppressed axon collateral arborization through inhibition of TrkB.

A, Co-immunoprecipitation and phosphotyrosine analysis in HEK293T cells co-transfected with TrkB-V5 and Mock, wild-type PTPRO-FLAG (WT), $PTPRO^{DA}$-FLAG (DA), or $PTPRO^{NTD}$-FLAG (NTD). TrkB-V5 immunoprecipitates (IP: V5) were immunoblotted for FLAG, V5, and phosphotyrosine (pTyr); input lysates were probed as indicated. ***B***, Quantification of phosphorylation levels (mean ± SEM), normalized to immunoprecipitated TrkB; n = 4 independent transfection experiments. One-way repeated-measures ANOVA with Geisser–Greenhouse correction followed by Tukey's multiple-comparisons test. *p < 0.05, **p < 0.01. ***C***, Representative P2 corticopontine projections after overexpression of Mock, TrkB, TrkB + wild-type PTPRO, or TrkB + $PTPRO^{DA}$. The white dashed line delineates the pons. Scale bar, 200 μm. ***D***, Quantification of the images in (***C***). n = 6 mice per group. Values are normalized to axon main shaft and shown as the mean ± SEM. One-way ANOVA followed by Tukey's multiple-comparisons test. *p < 0.05, **p < 0.01, ***p < 0.001. The mouse was used as the statistical unit. ***E***, Representative sparsely labeled and traced axons from Mock and TrkB groups. Red arrowheads mark collateral branch points, and the white dashed line delineates the pons. Scale bar, 100 μm. ***F***, Quantification of branch numbers at each branch order. ***G***, Quantification of the collateral complexity index for each mouse. ***H***, The region of the pons underneath the corticospinal axonal shaft was evenly divided into five bins along the dorsoventral axis. Quantification of branch numbers in each dorsoventral bin. ***F-H***, n = 5 mice per group. Values represent the mean ± SEM. Welch's t test or Mann–Whitney U test, depending on data normality and homogeneity of variance. *p < 0.05, **p < 0.01, ***p < 0.001. The mouse was used as the statistical unit. ***I***, Representative P2 corticopontine projections after transfection with sh*Scramble*, sh*Ptpro*, sh*Ntrk2*, or sh*Ptpro* + sh*Ntrk2*. Scale bar, 200 μm. ***J***, Quantification of fluorescence intensities in (***I***). n = 6 mice per group. Values are normalized to axon main shaft and shown as the mean ± SEM. One-way ANOVA followed by Tukey's multiple-comparisons test. *p < 0.05, **p < 0.01, ***p < 0.001. The mouse was used as the statistical unit.

Figure 7. The PTPRO-TrkB-PI3K signaling axis was essential for the regulation of axon collateral arborization.

JNeurosci Accepted Manuscript

A*,** Schematic illustration of the experimental design for intragastric administration. Mice electroporated at E12.5 received vehicle or the PI3K inhibitor BKM120 (buparlisib; 3 mg/kg) once daily at P0, P1, and P2 and were analyzed at P2. ***B, Representative P2 corticopontine projections from sh*Scramble* or sh*Ptpro* groups treated with vehicle or BKM120. The white dashed line delineates the pons, and the labeled tract is the axon main shaft. Scale bar, 200 μm. ***C***, Quantification of the images in (***B***). Fluorescence intensity in each bin was normalized to that of the axon main shaft. n = 6 mice per group. Values are normalized to axon main shaft and shown as the mean ± SEM. One-way ANOVA followed by Tukey's multiple-comparisons test. *p < 0.05, **p < 0.01, ***p < 0.001. The mouse was used as the statistical unit. ***D***, Representative sparsely labeled and traced axons from sh*Scramble* or sh*Ptpro* groups treated with vehicle or BKM120. Red arrowheads mark collateral branch points, and the white dashed line delineates the pons. Scale bar, 100 μm. ***E***, Quantification of the average number of branches per collateral. ***F***, Quantification of the collateral complexity index for each mouse. ***G***, Quantification of branch numbers at each branch order. ***H***, Quantification of branch numbers in each dorsoventral bin. ***E*-*H***, n = 6 mice per group. Values represent the mean ± SEM. Welch's one-way ANOVA followed by Tamhane's T2 test, Kruskal–Wallis test followed by Dunn's test or one-way ANOVA followed by Tukey's test, depending on data normality and homogeneity of variance. *p < 0.05, **p < 0.01, ***p < 0.001. The mouse was used as the statistical unit.

JNeurosci Accepted Manuscript

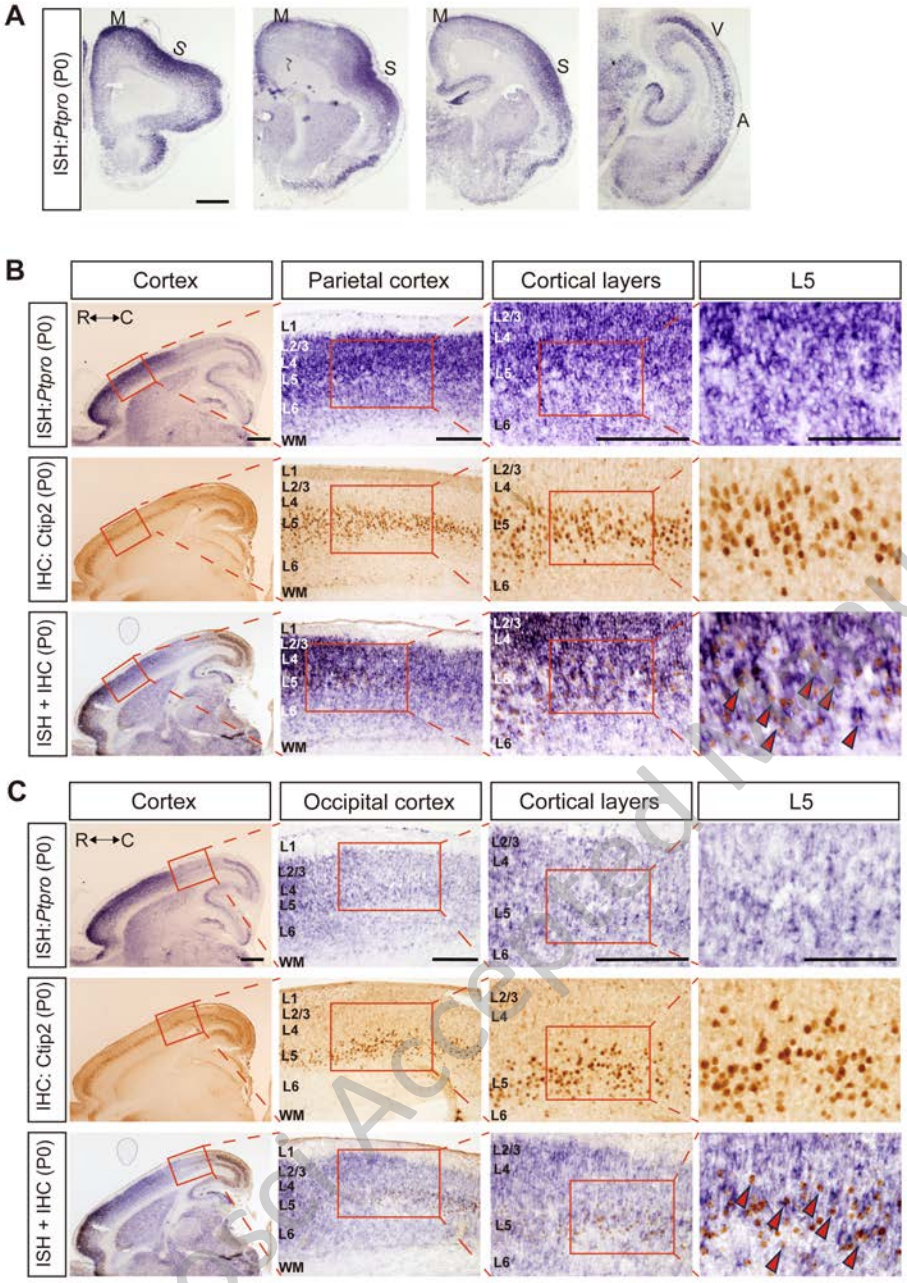

JNeurosci Accepted Manuscript

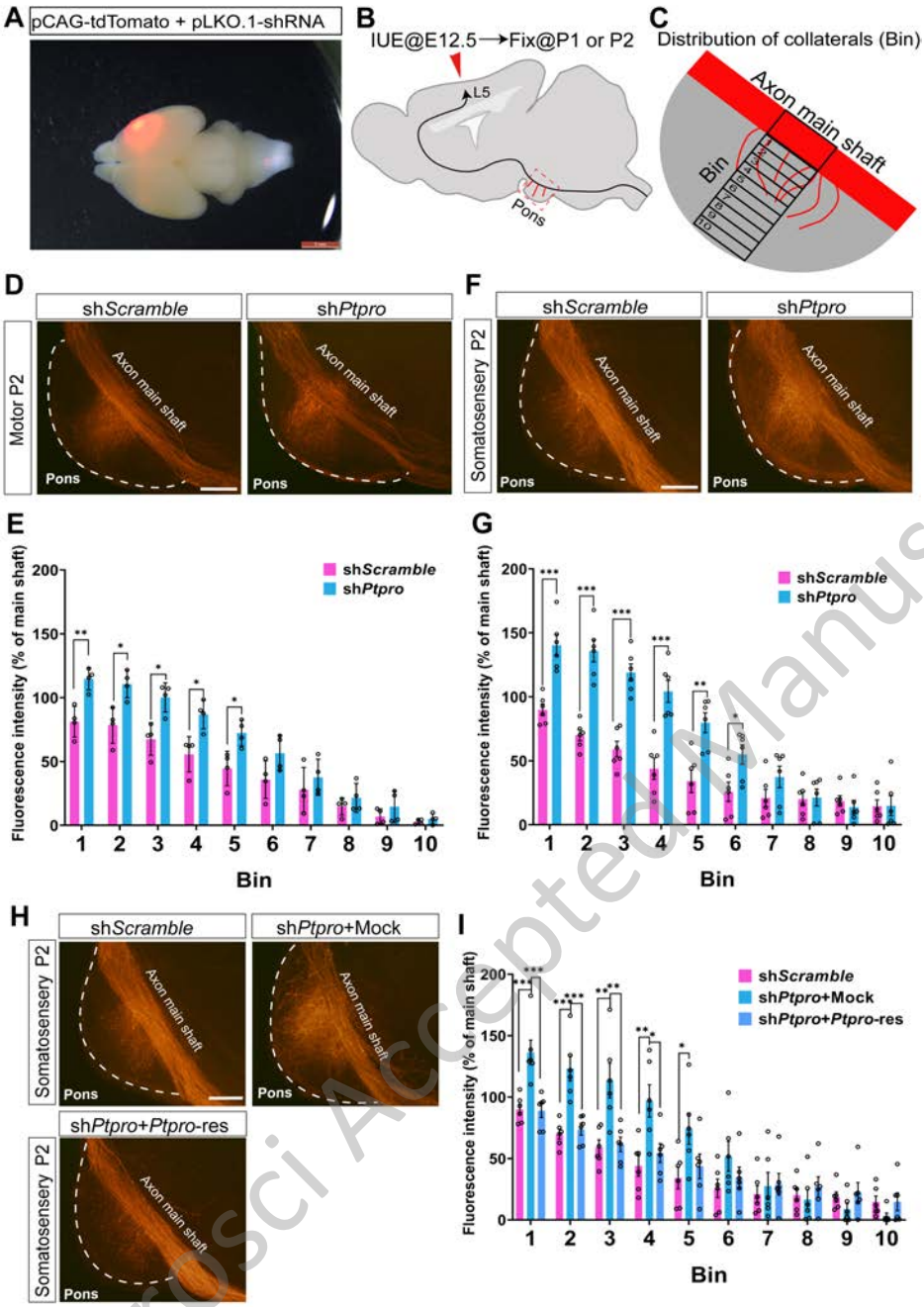

JNeurosci Accepted Manuscript

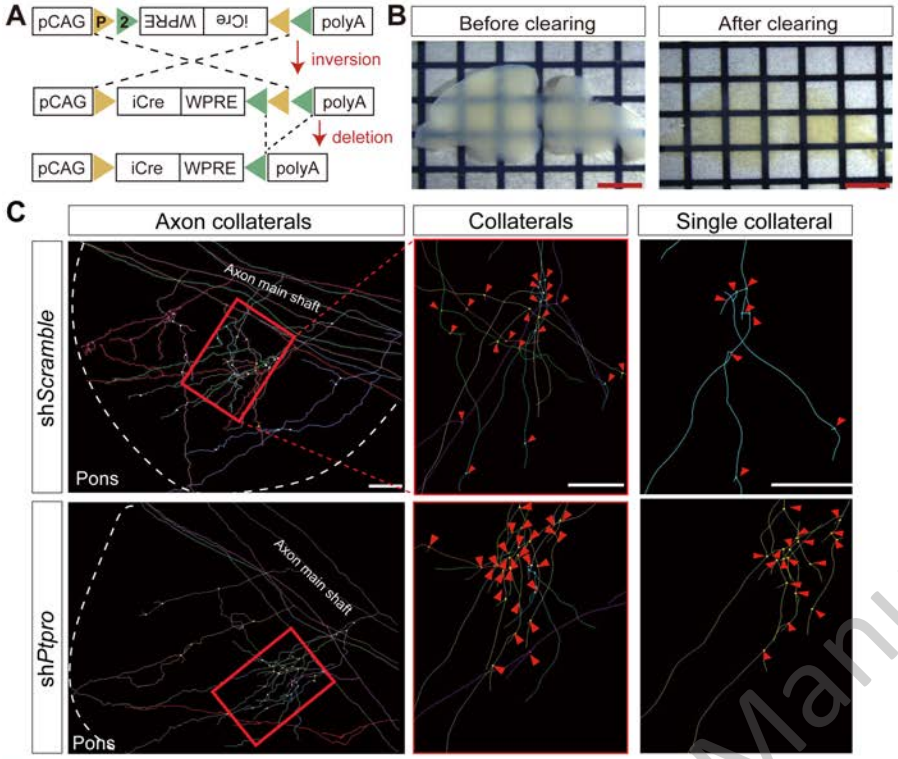

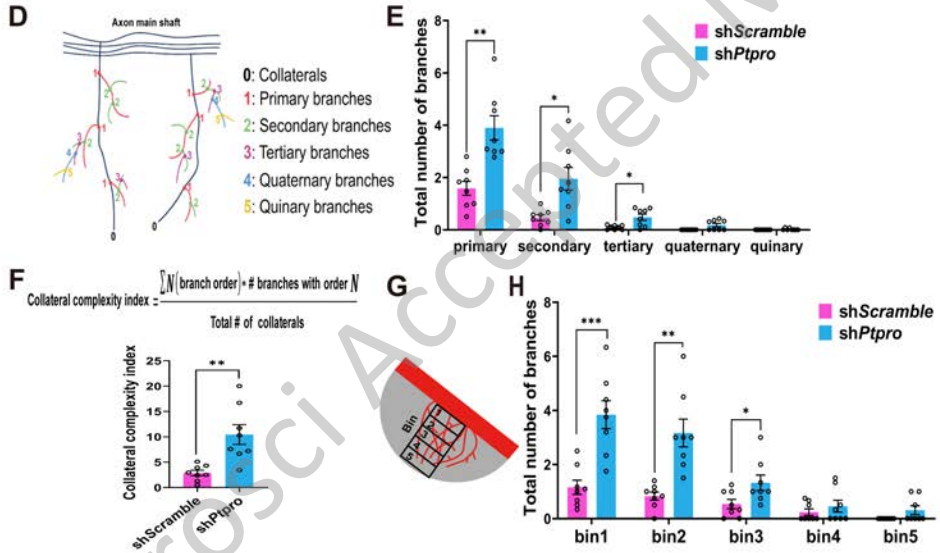

JNeurosci Accepted Manuscript

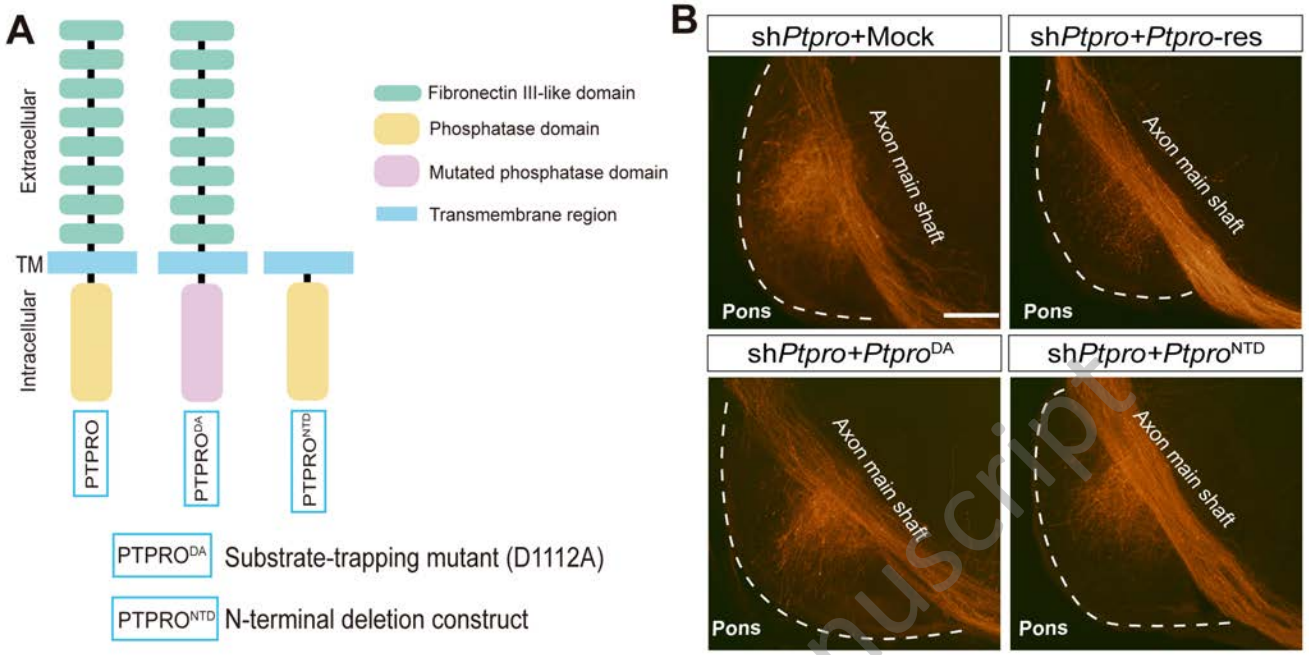

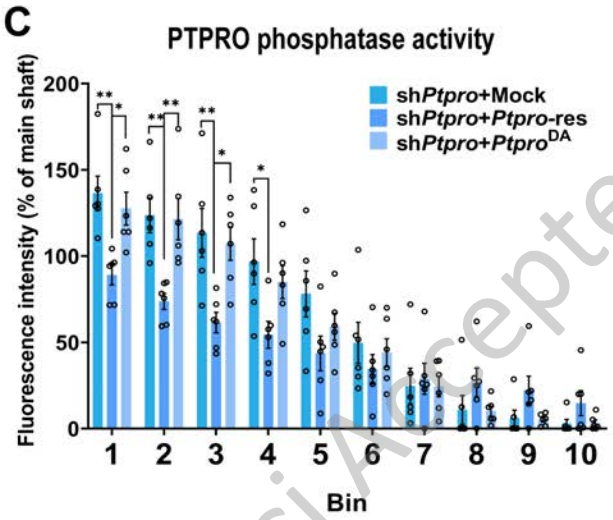

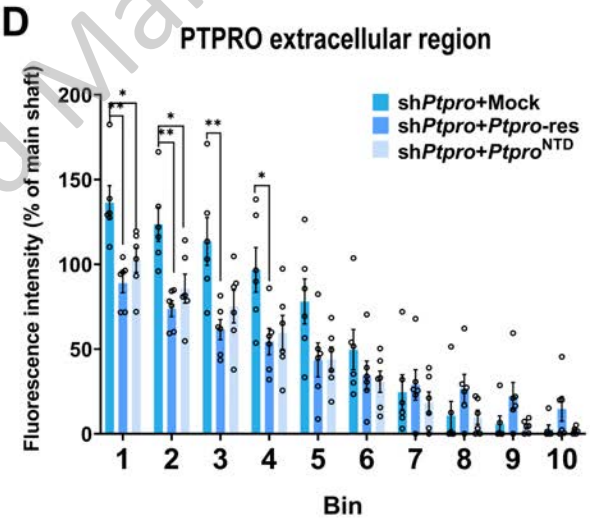

JNeurosci Accepted Manuscript

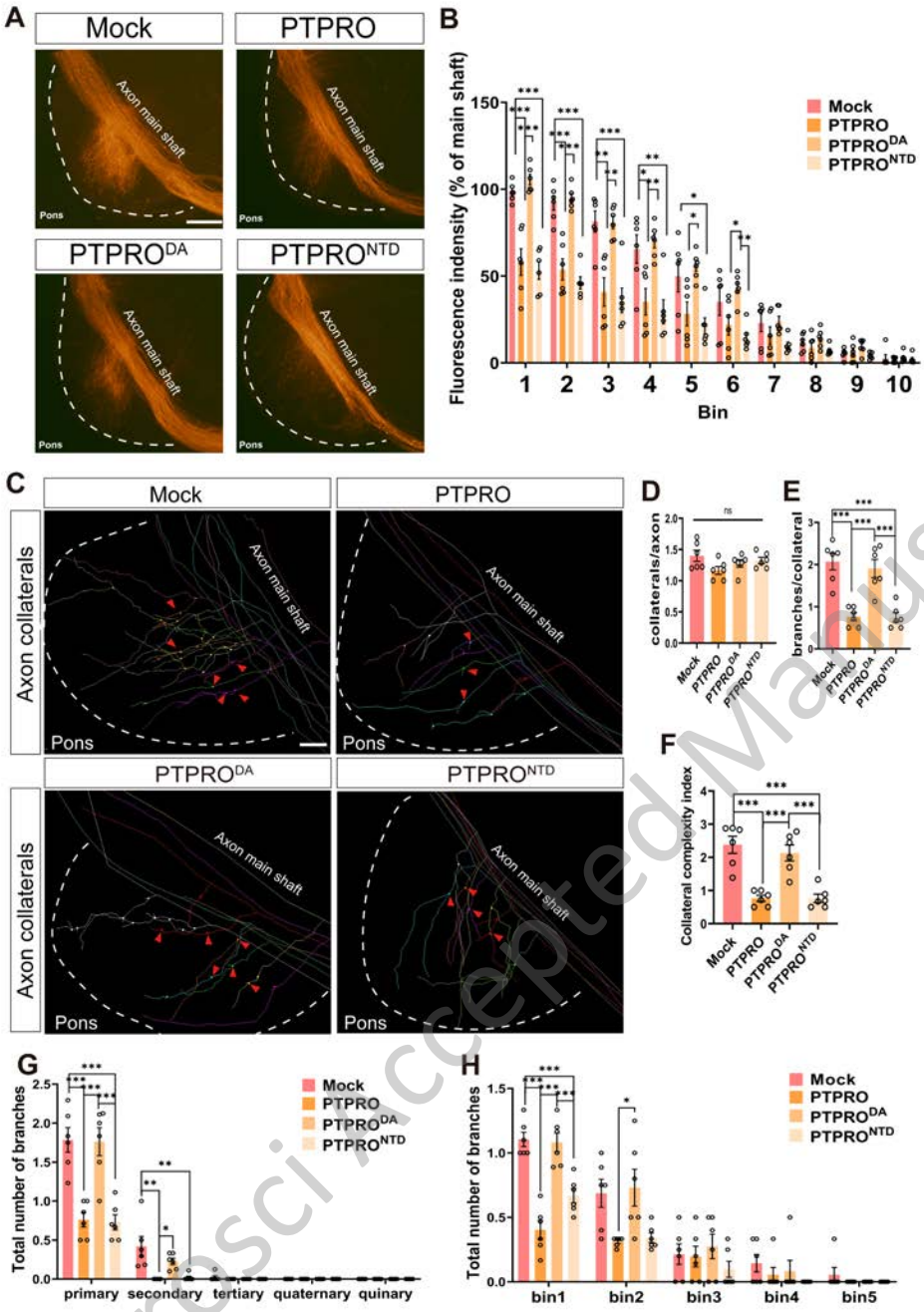

JNeurosci Accepted Manuscript

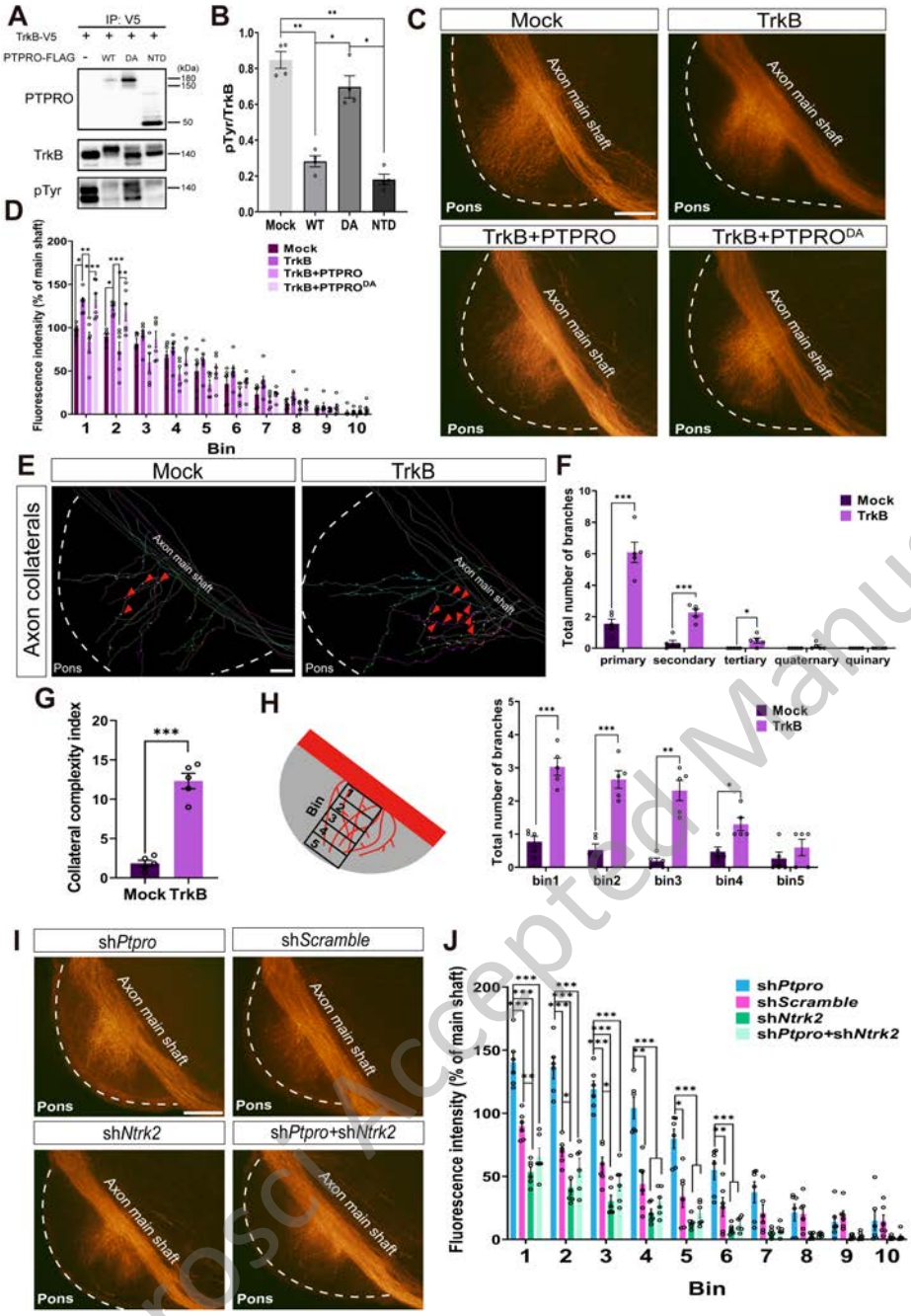

JNeurosci Accepted Manuscript

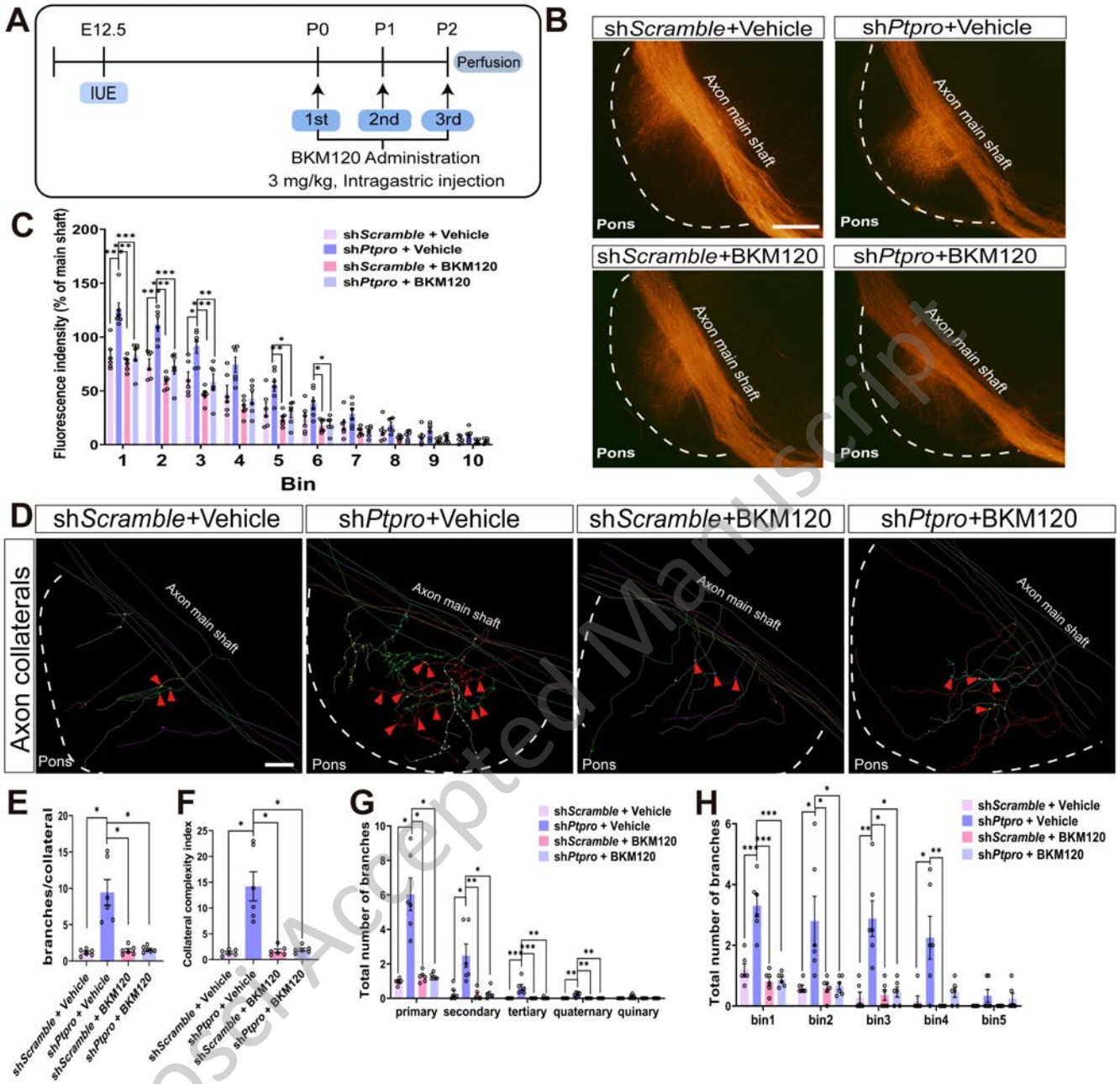

JNeurosci Accepted Manuscript